INVESTIGATION OF RADIATION-INDUCED INTERSTITIALS IN $RbCaF_3$

BY

ANOOSHIRVAN JAFARI

Bachelor of Science
Tehran University
Tehran, Iran
1966

Master of Science
Pahlavi University
Shiraz, Iran
1969

Master of Science
Indiana University
Bloomington, Indiana
1974

Submitted to the Faculty of the Graduate College
of the Oklahoma State University
in partial fulfillment of the requirements
for the Degree of
DOCTOR OF PHILOSOPHY
July, 1980

INVESTIGATION OF RADIATION-INDUCED

INTERSTITIALS IN $RbCaF_3$

Thesis Approved:

Larry E. Halliburton
Thesis Adviser

Timothy A Wilson

Paul W Westhaus

J Paul Goodyear

W. A. Sibley

Norman N Durham
Dean of the Graduate College

ACKNOWLEDGMENTS

The author wishes to express his appreciation to his major adviser, Dr. L. E. Halliburton for his guidance and assistance throughout this study. Appreciation is also expressed to the other committee members, Dr. W. A. Sibley, Dr. T. M. Wilson, Dr. P. A. Westhaus, and Dr. J. P. Devlin for their invaluable suggestions and discussions.

Appreciation is also extended to Dr. E. Sonder for supplying the $RbCaF_3$ crystals used in this study.

Special gratitude is expressed to my wife, Aghdass, for her understanding, encouragement, and assistance in typing this manuscript. Thanks are also extended to my daughter, Gita, and my son, Gooya, for their understanding and many sacrifices.

TABLE OF CONTENTS

LIST OF TABLES

LIST OF FIGURES

CHAPTER I

INTRODUCTION

Many important properties of crystals are controlled by defects. The color of many crystals is due to imperfections, thus explaining why many defects are called color centers. The conductivity of some semiconductors is due entirely to chemical impurities and the luminescence of crystals is nearly always connected with the presence of impurities. Diffusion of atoms may be accelerated enormously by the presence of vacancies and the mechanical and plastic properties are usually controlled by imperfections.

Real solids contain both "point defects" and "extended defects". In this study we will be concerned with the point defects in a simple fluoride material. The simplest of all point defects are isolated interstitials and vacancies. The interstitial is an atom that occupies a position where no atom would exist in the perfect crystal, and the vacancy is where an atom is missing from the perfect crystal. Different point defects are usually identified by a letter. For example, a negative ion vacancy is called an F center and a split-interstitial, where two atoms or ions share one lattice site, is called an H center.

Defects can also be classified as "intrinsic" or "extrinsic". In the case of intrinsic defects, we are involved only with the atoms of the perfect solid. Extrinsic defects correspond to cases where impurity atoms are also involved in the defect. For example, the H center is

an intrinsic defect while the impurity-associated interstitial, called the H_A center, is an extrinsic defect. Another intrinsic well-characterized defect in halide materials is the self-trapped hole center, also known as a V_k or $[X_2^-]$ center. It consists of two halide ions sharing a hole (missing an electron) and forming a diatomic molecular ion. The two halide ions are displaced from their normal lattice sites so as to have a smaller spacing than the normal negatively-charged halide ions. A more complete review of different kinds of defects is given by Sonder and Sibley (1).

Different techniques have been used to study point defects, one of their main objectives being to establish models for the structure of these defects, which, after careful examination and perfection, might ultimately yield a consistent description of all their physical properties. Point defects in solids usually have a number of electronic states between which optical transitions are possible. Therefore the most obvious effect of defects is usually on the optical properties of the solid and, because of this, optical techniques are the ones through which an initial study of point defects is often made.

Magnetic and electric techniques are also of fundamental importance in the determination of defect structure. Two powerful methods of this type are ESR (electron spin resonance) and ENDOR (electron-nuclear double resonance). A simple ESR expriment consists of inducing transitions between spin states which have been split in energy by an applied magnetic field. The mere observation of an ESR spectrum indicates that the center has at least one unpaired electron, but much more information is found through "g values" and "hyperfine interactions" (2). In order to determine the interactions of the defect electron with the nuclei in

shells beyond the nearest and next nearest neighbors, ENDOR techniques, which have much better resolution, are used (3).

Mechanical and thermal properties of solids can also be changed significantly by the presence of defects and this provides additional techniques to study defects. The volume changes that accompany defect production in alkali halides have been measured by several techniques (4). In conjunction with measurements of lattice parameters, they have been the major tool in deciding whether irradiation of alkali halides produced only vacancies or vacanies plus interstitials. If we try to measure the lattice parameters of a crystal containing defects by x-ray scattering, the main Bragg diffraction peak will be shifted due to the defects. Additional information can be obtained about the strength and symmetry of the defect's strain fields due to the distortion and bending of the lattice planes in their vicinity. Measurements have shown that the irradiation of crystals can increase their flow stress. This suggests that defects introduced by irradiation are in some way active in hardening crystals. The contribution of various type of defects to this hardening is different (4). Therefore, this phenomena can give us information about the nature of defects present in the crystals.

Considering the thermal properties, the introduction of defects can change both the specific heat and the thermal conductivity of crystals. In practice, neither is significantly changed by the concentration of defects normally achievable in ionic solids at room temperature and only thermal conductivity studies at low temperatures have proved a useful tool.

One of the questions in the study of radiation damage to materials is the processes and mechanisms which leads to the creation of a defect.

The mechanisms by which defects can be produced by radiation in ionic solids are (1): electronic processes, elastic collisions, and radiolysis (photochemical mechanisms). The electronic processes include those in which an electronic state is changed or charge is moved about by the absorption of radiant energy, but in which no ionic or atomic defects are formed. Elastic collision processes are those in which atoms or ions are displaced due to momentum and energy transfer from irradiating particles. Radiolysis are those processes in which atomic or ionic defects are produced by a series of reactions beginning with an electronic excitation.

In our study, we will be dealing with ionic defects. Therefore, their production will be discussed in more detail. If we irradiate a crystal with energetic particles such as electrons, protons, or neutrons, they occasionally undergo elastic collisions with the nuclei of lattice atoms or ions. Calculations show (4) that the maximum amount of kinetic energy T_m which can be transferred from the incident particle to a lattice ion is:

$$T_m = \frac{4 M_1 M_2 E (1 + E / 2 M_1 C^2)}{(M_1 + M_2)^2} \qquad (1)$$

where E and M_1 are the energy and mass of the incident particle and M_2 is the mass of the lattice ion. It is clear that in elastic collisions, heavy particles can transfer more energy than the light ones, and a certain minimum amount of energy is needed for a lattice ion to be displaced. Therefore, in a collision, if T_m is less than this minimum energy, no elastic collision radiation damage will occur or the damage rate will be strongly energy dependent.

The elastic collision mechanism can not explain the production of interstitial-vacancy pairs (Frenkel pairs) by ultraviolet light, because these photons can not transfer sufficient momentum to lattice ions to displace them. In such cases it is found that the radiolysis process is capable of creating lattice defects. In this process at least the following three stages must be identifiable (4). First, an electronic excitation must occur, resulting, at least momentarily, in creation of an electronic defect in the lattice. Second, the energy of the electronic defect must be converted into kinetic energy of a lattice ion in such a way that the ion is ejected from its normal site. Third, a route must exist for this lattice ion to move sufficiently far from its associated vacancy that a stable defect is formed.

Interstitial atoms or H centers, were first characterized by the ESR studies of Kanzig and Woodruff (5). These result were supported by the optical studies of Compton and Klick (6) which showed that H centers were produced at low temperatures in proportion to the number of F centers formed and that this production takes place simultaneously. Later the combination of flow stress and optical measurements (7, 8, 9) and especially the lattice measurements (10, 11) provided convincing evidence that Frenkel pair production by x rays occured at all radiation temperatures.

Despite this accumulated evidence for the existance of Frenkel pairs, their production mechanism was still not clear. However, additional observations (12, 13, 14) led to the so-called Pooley-Hersh mechanism, in which the production of Frenkel pairs was associated with the non-radiative recombination of electrons with self-trapped hole centers created by the radiation. The evidence for this conclusion was Pooley's

observations (15) that the F center production efficiency was dependent on whether electron - hole recombination luminesence occurred or not. When this emission occured, F center production decreased. A way in which H centers and F centers separate was also postulated by Pooley (16). He said because of the [110] orientation of the self-trapped hole center, the nonradiative recombination transition causes the two halide ions to be thrown apart along the [110] direction, roughly sharing the recombination energy and causing an anion replacement collision sequence to propagate along the close-packed halide row. There have been several investigation concerning H centers (17, 18) in alkali halides since the original report. Other investigations have described the H_A center in alkali halides (19, 20, 21, 22). Figure 1(b) and Figure 2(b) show the H and H_A centers in KCl. Radiation damage in more complex halide crystals such as the provskite $KMgF_3$ has been studied (23). It was found that the radiolysis process dominates in this material.

ESR studies of intrinsic (H) and impurity-associated (H_A) flourine interstitials have been done in $KMgF_3$ (24, 25). The intrinsic H center in $KMgF_3$ shown in Figure 1(a) is somewhat similar to that in KCl. The orientation of the molecular-ion axis is approximately halfway between the [100] and [110] directions in the (001) plane containing the magnesium ion. There is small but significant interaction between the unpaired hole and the nuclei of the two adjacent fluorine ions located along the [110] directions. The $KMgF_3$ H_A centers shown in Figure 2(a), are the result of an interstitial fluorine atom combining with two neighboring lattice fluorine ions to form a molecular ion stabilized adjacent to an unidentified impurity. It is also found that the H_A center undergoes rapid motion about the neighboring impurity ion.

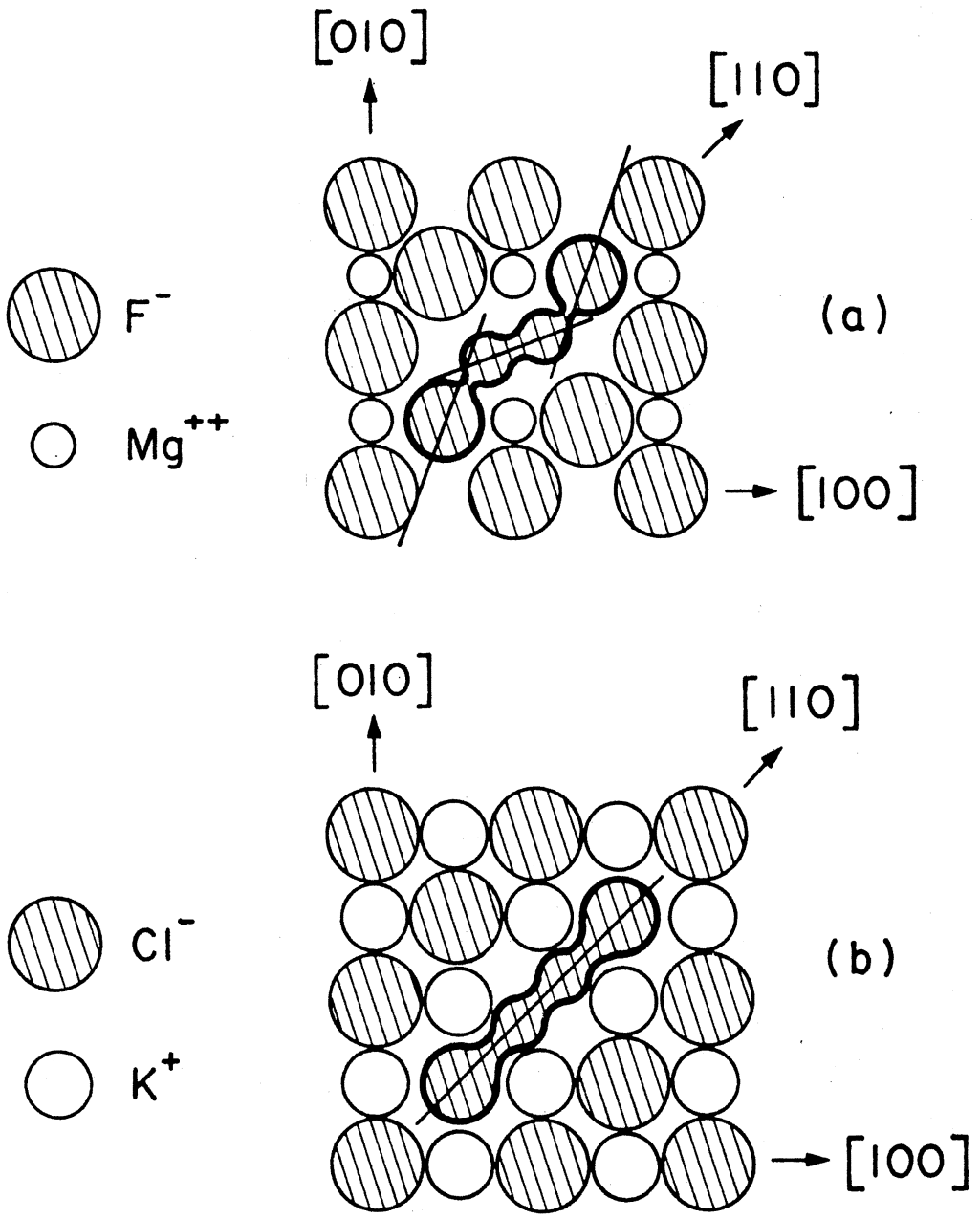

Figure 1. H Center in $KMgF_3$ (a), and H Center in KCl (b)

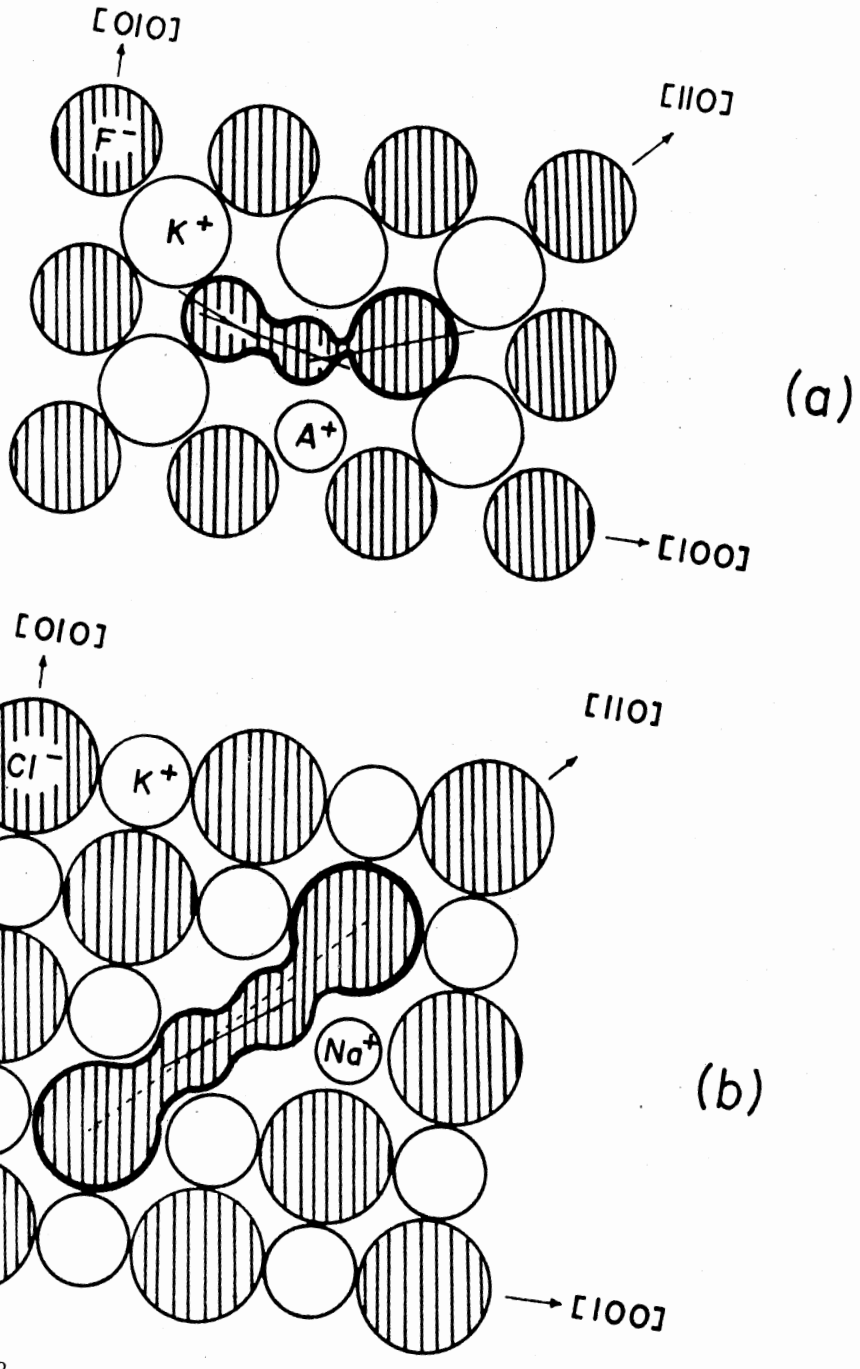

Figure 2. H_A Center in $KMgF_3$ (a), and H_A Center in KCl (b)

Crystal Structure of $RbCaF_3$

Single crystals of $RbCaF_3$ are found to have cubic perovskite structure at room temperature which is shown in Figure 3. Modine, Sonder and Unruh (26) have reported a lower symmetry for $RbCaF_3$ at temperatures below 198 K. From birefringence measurements and ESR studies of the Fe^{3+} impurity, they found that the crystal transforms to a tetragonal structure at 198 K. This phase transition was near second order and at lower temperatures, a well-defined domain structure was revealed. From dielectric function and specific heat anomalies measurements, it was found that other phase transitions occur at about 43 K and 10 K. Bates, Major, and Modine (27) have reported the results of optical birefringence, Raman scattering, and neutron scattering measurements which show the cubic-to-tetragonal phase change is at 196 K. Also, a very slow transition to a lower symmetry structure was observed at 42 K. Ho and Unruh (28) have reported phase changes at 198 K, 42 K, and 7 K from specific heat measurements. The ESR studies of V_k centers in a single domain $RbCaF_3$ crystal at 77 K by Halliburton and Sonder (29) show the twisting of CaF_6 octahedron about the tetragonal axis as a result of the 196 K phase change. The amount of twisting at 77 K was found to be 7.1^{o}. Maetz, Mullner, and Jex (30) have reported x-ray diffraction experiments on the domain structure of $RbCaF_3$. From the three orthogonal domains which are possible, as the temperature is lowered below the phase transition at 198 K, the relative volume of the domain varies, one group increases and the other two groups decrease. Seretlo, Martin and Sonder (31) have studied the optical absorption of radiation-induced defects in $RbCaF_3$ at 80 K and liquid helium temperature. They reported absorption bands at 320, 400 and 530nm, but could not make definite assign-

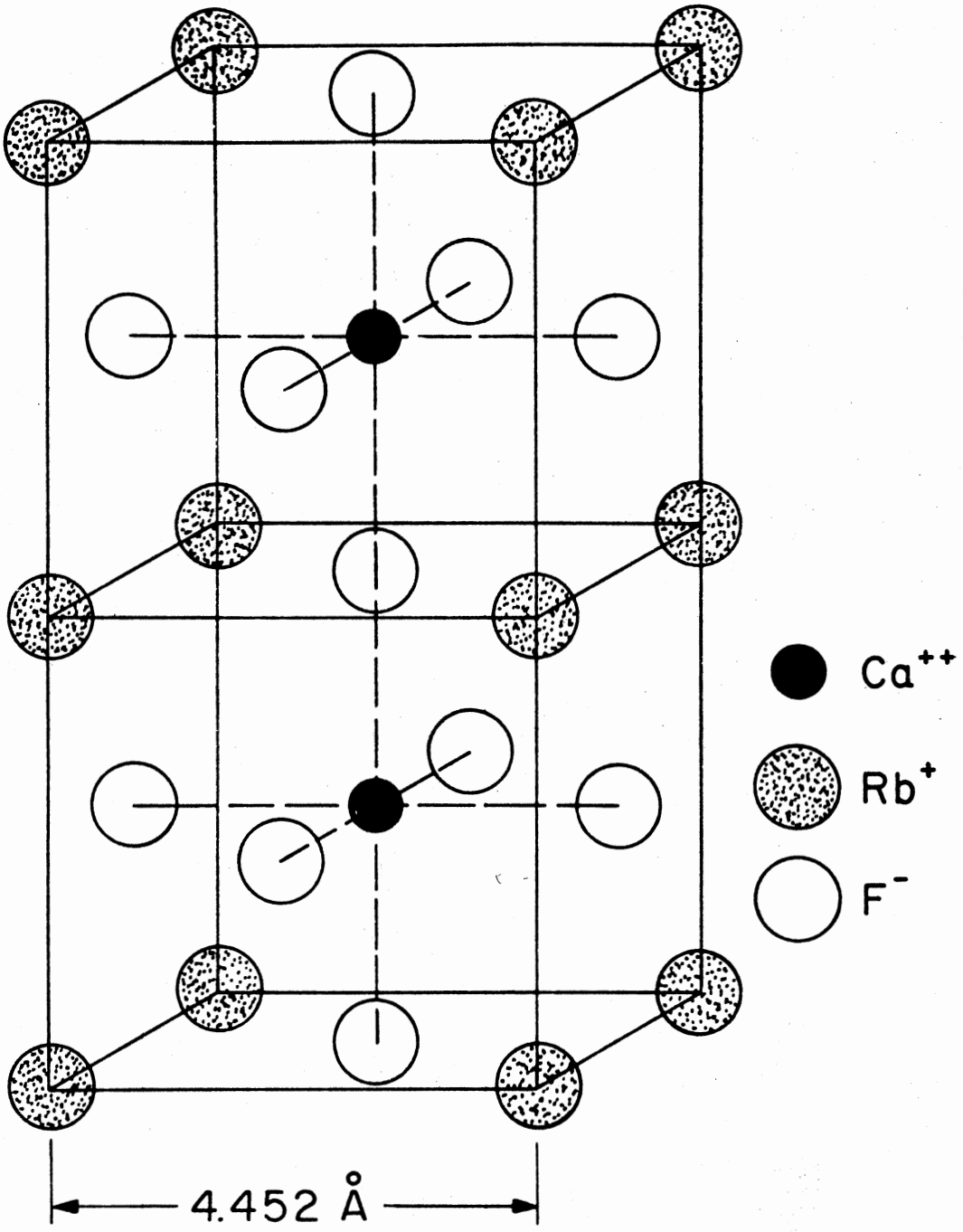

Figure 3. Crystal Structure of $RbCaF_3$

ments. They have mentioned the possibility of the 320nm band being due to V_k, H, H_A, and F centers and the 530nm band due to an electron trapping center. Burris (32), in an ESR study of the H center in $RbCaF_3$, found that the defect is composed of two fluorine atoms, preferentially aligned along the axis of rotation of the CaF_6 octahedra.

Purpose of This Investigation

In this study H centers are produced in $RbCaF_3$ by electron irradiation at 77 K. Using ESR spectra, the structure of these H centers is determined. From thermal anneal studies, we get information about the stability of the H centers and their conversion into impurity-associated interstitial centers (H_A). Again using ESR spectra, we determine the structure of these H_A centers. Since the lattice parameter of $RbCaF_3$ is larger than $KMgF_3$, this work provides the opportunity to see the effect of increase in the distance between neighboring ions on the structure of H and H_A centers. We will also correlate our results with the optical measurements of Seretlo, Martin, and Sonder (31), and derive more specific conclusions about the nature of the optical bands produced in $RbCaF_3$ by irradiation.

CHAPTER II

THEORY AND ANALYSIS

The general spin Hamiltonian, for the case when the unpaired electron interacts only with two nuclei, can be written as

$$H = \beta . \vec{S} . \overleftrightarrow{g} . \vec{H} + \vec{I}_1 . \overleftrightarrow{A}_1 . \vec{S} + \vec{I}_2 . \overleftrightarrow{A}_2 . \vec{S} - g_N \beta_N \vec{H} . (\vec{I}_1 + \vec{I}_2) \qquad (2)$$

where β is the Bohr magneton, $\vec{S}$ is the spin operator for the unpaired electron, $\overleftrightarrow{g}$ is the g-tensor for the system, $\vec{H}$ is the external magnetic field, $\vec{I}_1$ and $\vec{I}_2$ are the nuclear spin operators for the two nuclei involved, $\overleftrightarrow{A}_1$ and $\overleftrightarrow{A}_2$ are the hyperfine tensors representing the dipole-dipole and Fermi contact interaction of the two nuclei with the spin of the unpaired electron, g_N is the nuclear g factor, and β_N is the nuclear magneton. In Equation (2), the first term is the electronic Zeeman, the next two terms represent the hyperfine interaction, and the last term is the nuclear Zeeman interaction.

The spin Hamiltonian is used to describe the ESR spectra, i.e., the spin Hamiltonian parameters are obtained from the angular dependence of the ESR spectra. After their "best" values have been determined, the hyperfine parameters can be related to the unpaired electron's wavefunction by the following expressions.

$$A_{ij} = a + B_{ij}$$

$$a = (8/3)\, \pi\, g\, \beta\, g_N\, \beta_N\, |\, \psi(0)|^2$$

$$B_{ij} = g\ \beta\ g_N\ \beta_N \int |(3X_iX_j/r^5) - (\delta_{ij}/r^3)||\psi(r)|^2 dv$$

In order to use the spin Hamiltonian to determine the g tensor and hyperfine tensor parameters from the ESR spectra, we must write it in a form suitable for computation. First, the spin Hamiltonian must be expressed in terms of the individual tensor's principal axis coordinate systems. Then, each of these coordinate systems must be transformed into a common magnetic-field coordinate system, that is, one which has the magnetic field always along its Z-axis. Once the spin Hamiltonian is expressed in a single coordinate system, it can be written in matrix form and diagonalized. It is the resulting eigenvalues that can be directly compared to the experimental ESR spectra.

To begin this process of rewriting the spin Hamiltonian in a form suitable for computation, let us define the following coordinate systems.

(x_0,y_0,z_0): Principal axes of the $\overleftrightarrow{g}$ tensor.

(x_1,y_1,z_1): Principal axes of the $\overleftrightarrow{A}_1$ tensor.

(x_2,y_2,z_2): Principal axes of the $\overleftrightarrow{A}_2$ tensor.

(x_c,y_c,z_c): Crystal axes.

(x,y,z): Magnetic field coordinate system, chosen such that the z-axis is along the magnetic field.

In the various principal coordinate systems, the spin Hamiltonian becomes

$$H = S_{x_0}\ g_x\ H_{x_0} + S_{y_0}\ g_y\ H_{y_0} + S_{z_0}\ g_z\ H_{z_0} + I^1_{x_1}\ A^1_x\ S_{x_1}$$
$$+ I^1_{y_1}\ A^1_y\ S_{y_1} + I^1_{z_1}\ A^1_z\ S_{z_1} + I^2_{x_2}\ A^2_x\ S_{x_2} + I^2_{y_2}\ A^2_y\ S_{y_2}$$
$$+ I^2_{z_2}\ A^2_z\ S_{z_2} - g_N\beta_N\ H\ (\ I^1_z + I^2_z\ ).$$

The superscripts on the nuclear spin operators I and the hyperfine parameters A denote nucleus 1 and nucleus 2, respectively. To write the spin Hamiltonian in the magnetic field coordinate system, the following coordinate transformation matrices are used:

$[TG]$: Transforms the principal axes of the $\overleftrightarrow{g}$ tensor to the crystal axes.

$[T1]$: Transforms the principal axes of the $\overleftrightarrow{A}_1$ tensor to the crystal axes.

$[T2]$: Transforms the principal axes of the $\overleftrightarrow{A}_2$ tensor to the crystal axes.

$[R]$: Transforms the crystal coordinate system to the magnetic coordinate system.

$[TRG] = [TG][R]$: Transforms the principal axes of the $\overleftrightarrow{g}$ tensor to the magnetic coordinate system.

$[TR1] = [T1][R]$: Transforms the principal axes of the $\overleftrightarrow{A}_1$ tensor to the magnetic coordinate system.

$[TR2] = [T2][R]$: Transforms the principal axes of the $\overleftrightarrow{A}_2$ tensor to the magnetic coordinate system.

Therefore we can write:

$$\begin{pmatrix} x_0 \\ y_0 \\ z_0 \end{pmatrix} = [TRG] \begin{pmatrix} x \\ y \\ z \end{pmatrix}$$

$$\begin{pmatrix} x_1 \\ y_1 \\ z_1 \end{pmatrix} = [TR1] \begin{pmatrix} x \\ y \\ z \end{pmatrix}$$

$$\begin{pmatrix} x_2 \\ y_2 \\ z_2 \end{pmatrix} = [\,TR2\,] \begin{pmatrix} x \\ y \\ z \end{pmatrix}$$

The spin operators, $\vec{S}$ and $\vec{I}$, must transform in same manner as the coordinates. For example:

$$S_{x_0} = TRG(1,1)\ S_x + TRG(1,2)\ S_y + TRG(1,3)\ S_z$$

$$S_{y_0} = TRG(2,1)\ S_x + TRG(2,2)\ S_y + TRG(2,3)\ S_z$$

$$S_{z_0} = TRG(3,1)\ S_x + TRG(3,2)\ S_y + TRG(3,3)\ S_z$$

$$H_{x_0} = TRG(1,3)\ H$$

$$H_{y_0} = TRG(2,3)\ H$$

$$H_{z_0} = TRG(3,3)\ H$$

Using the transformations, the spin Hamiltonian takes the following form.

$$\begin{aligned} H = {} & \beta H g_x [\, TRG(1,3)\ TRG(1,1)\ S_x + TRG(1,3)\ TRG(1,2)\ S_y \\ & + TRG(1,3)\ TRG(1,3)\ S_z\,] \\ & + \beta H g_y [\, TRG(2,3)\ TRG(2,1)\ S_x + TRG(2,3)\ TRG(2,2)\ S_y \\ & + TRG(2,3)\ TRG(2,3)\ S_z] \\ & + \beta H g_z [\, TRG(3,3)\ TRG(3,1)\ S_x + TRG(3,3)\ TRG(3,2)\ S_y \\ & + TRG(3,3)\ TRG(3,3)\ S_z] \end{aligned}$$

$$
\begin{aligned}
&+ A_x^1 \,[\mathrm{TR1}(1,1)\ \mathrm{TR1}(1,1)\ I_x^1 S_x + \mathrm{TR1}(1,1)\ \mathrm{TR1}(1,2)\ I_x^1 S_y \\
&\quad + \mathrm{TR1}(1,1)\ \mathrm{TR1}(1,3)\ I_x^1 S_z + \mathrm{TR1}(1,2)\ \mathrm{TR1}(1,1)\ I_y^1 S_x \\
&\quad + \mathrm{TR1}(1,2)\ \mathrm{TR1}(1,2)\ I_y^1 S_y + \mathrm{TR1}(1,2)\ \mathrm{TR1}(1,3)\ I_y^1 S_z \\
&\quad + \mathrm{TR1}(1,3)\ \mathrm{TR1}(1,1)\ I_z^1 S_x + \mathrm{TR1}(1,3)\ \mathrm{TR1}(1,2)\ I_z^1 S_y \\
&\quad + \mathrm{TR1}(1,3)\ \mathrm{TR1}(1,3)\ I_z^1 S_z] \\
&+ A_y^1 \,[\mathrm{TR1}(2,1)\ \mathrm{TR1}(2,1)\ I_x^1 S_x + \mathrm{TR1}(2,1)\ \mathrm{TR1}(2,2)\ I_x^1 S_y \\
&\quad + \mathrm{TR1}(2,1)\ \mathrm{TR1}(2,3)\ I_x^1 S_z + \mathrm{TR1}(2,2)\ \mathrm{TR1}(2,1)\ I_y^1 S_x \\
&\quad + \mathrm{TR1}(2,2)\ \mathrm{TR1}(2,2)\ I_y^1 S_y + \mathrm{TR1}(2,2)\ \mathrm{TR1}(2,3)\ I_y^1 S_z \\
&\quad + \mathrm{TR1}(2,3)\ \mathrm{TR1}(2,1)\ I_z^1 S_x + \mathrm{TR1}(2,3)\ \mathrm{TR1}(2,2)\ I_z^1 S_y \\
&\quad + \mathrm{TR1}(2,3)\ \mathrm{TR1}(2,3)\ I_z^1 S_z] \\
&+ A_z^1 \,[\mathrm{TR1}(3,1)\ \mathrm{TR1}(3,1)\ I_x^1 S_x + \mathrm{TR1}(3,1)\ \mathrm{TR1}(3,2)\ I_x^1 S_y \\
&\quad + \mathrm{TR1}(3,1)\ \mathrm{TR1}(3,3)\ I_x^1 S_z + \mathrm{TR1}(3,2)\ \mathrm{TR1}(3,1)\ I_y^1 S_x \\
&\quad + \mathrm{TR1}(3,2)\ \mathrm{TR1}(3,2)\ I_y^1 S_y + \mathrm{TR1}(3,2)\ \mathrm{TR1}(3,3)\ I_y^1 S_z \\
&\quad + \mathrm{TR1}(3,3)\ \mathrm{TR1}(3,1)\ I_z^1 S_x + \mathrm{TR1}(3,3)\ \mathrm{TR1}(3,2)\ I_z^1 S_y \\
&\quad + \mathrm{TR1}(3,3)\ \mathrm{TR1}(3,3)\ I_z^1 S_z\,] \\
&+ \text{similar terms for } \vec{I}_2 . \overleftrightarrow{A}_2 . \vec{S} \\
&- g_N \beta_N H \,(I_z^1 + I_z^2)
\end{aligned}
$$

The spin Hamiltonian can be simplified as follows.

$$
\begin{aligned}
H = {} & W1\ S_x + W2\ S_y + W3\ S_z \\
& + W4\ I_x^1 S_x + W5\ I_x^1 S_y + W6\ I_x^1 S_z \\
& + W5\ I_y^1 S_x + W7\ I_y^1 S_y + W8\ I_y^1 S_z \\
& + W6\ I_z^1 S_x + W8\ I_z^1 S_y + W9\ I_z^1 S_z \\
& + W10\ I_x^2 S_x + W11\ I_x^2 S_y + W12\ I_x^2 S_z \\
& + W11\ I_y^2 S_x + W13\ I_y^2 S_y + W14\ I_y^2 S_z \\
& + W12\ I_z^2 S_x + W14\ I_z^2 S_y + W15\ I_z^2 S_z \\
& - g_N \beta_N H\ (I_z^1 + I_z^2)
\end{aligned}
$$

where

$$W1 = \beta H \left[g_x\ TRG(1,3)\ TRG(1,1) + g_y\ TRG(2,3)\ TRG(2,1) + g_z\ TRG(3,3)\ TRG(3,1) \right]$$

$$W2 = \beta H \left[g_x\ TRG(1,3)\ TRG(1,2) + g_y\ TRG(2,3)\ TRG(2,2) + g_z\ TRG(3,3)\ TRG(3,2) \right]$$

$$W3 = \beta H \left[g_x\ TRG(1,3)\ TRG(1,3) + g_y\ TRG(2,3)\ TRG(2,3) + g_z\ TRG(3,3)\ TRG(3,3) \right]$$

$$W4 = A_x^1\ TR1(1,1)\ TR1(1,1) + A_y^1\ TR1(2,1)\ TR1(2,1) + A_z^1\ TR1(3,1)\ TR1(3,1)$$

$$W5 = A_x^1\ TR1(1,1)\ TR1(1,2) + A_y^1\ TR1(2,1)\ TR1(2,2) + A_z^1\ TR1(3,1)\ TR1(3,2)$$

$$W6 = A_x^1\ TR1(1,1)\ TR1(1,3) + A_y^1\ TR1(2,1)\ TR1(2,3) + A_z^1\ TR1(3,1)\ TR1(3,3)$$

$$W7 = A_x^1\ TR1(1,2)\ TR1(1,2) + A_y^1\ TR1(2,2)\ TR1(2,2) + A_z^1\ TR1(3,2)\ TR1(3,2)$$

$$W8 = A_x^1\ TR1(1,2)\ TR1(1,3) + A_y^1\ TR1(2,2)\ TR1(2,3) + A_z^1\ TR1(3,2)\ TR1(3,3)$$

$$W9 = A_x^1 \, TR1(1,3) \, TR1(1,3) + A_y^1 \, TR1(2,3) \, TR1(2,3) + A_z^1 \, TR1(3,3) \, TR1(3,3)$$

$$W10 = A_x^2 \, TR2(1,1) \, TR2(1,1) + A_y^2 \, TR2(2,1) \, TR2(2,1) + A_z^2 \, TR2(3,1) \, TR2(3,1)$$

$$W11 = A_x^2 \, TR2(1,1) \, TR2(1,2) + A_y^2 \, TR2(2,1) \, TR2(2,2) + A_z^2 \, TR2(3,1) \, TR2(3,2)$$

$$W12 = A_x^2 \, TR2(1,1) \, TR2(1,3) + A_y^2 \, TR2(2,1) \, TR2(2,3) + A_z^2 \, TR2(3,1) \, TR2(3,3)$$

$$W13 = A_x^2 \, TR2(1,2) \, TR2(1,2) + A_y^2 \, TR2(2,2) \, TR2(2,2) + A_z^2 \, TR2(3,2) \, TR2(3,2)$$

$$W14 = A_x^2 \, TR2(1,2) \, TR2(1,3) + A_y^2 \, TR2(2,2) \, TR2(2,3) + A_z^2 \, TR2(3,2) \, TR2(3,3)$$

$$W15 = A_x^2 \, TR2(1,3) \, TR2(1,3) + A_y^2 \, TR2(2,3) \, TR2(2,3) + A_z^2 \, TR2(3,3) \, TR2(3,3)$$

Using the raising and lowering operators

$$S_+ = S_x + iS_y \quad , \quad S_- = S_x - iS_y$$

$$I_+ = I_x + iI_y \quad , \quad I_- = I_x - iI_y$$

or, equivalently,

$$S_x = \frac{1}{2} (S_+ + S_-), \; S_y = \frac{1}{2i} (S_+ - S_-)$$

$$I_x = \frac{1}{2} (I_+ + I_-), \; I_y = \frac{1}{2i} (I_+ - I_-)$$

we get

$$H = \frac{1}{2} (W1 - i\,W2) \, S_+ + \frac{1}{2} (W1 + i\,W2) \, S_- + W3 \, S_z$$

$$+ \frac{1}{4} (W4 - i\,W5 - i\,W5 - W7) \, I_+^1 \, S_+$$

$$+ \frac{1}{4} (W4 + i\,W5 - i\,W5 + W7) \, I_+^1 \, S_-$$

$$+ \frac{1}{4} (W4 - i\,W5 + i\,W5 + W7) \, I_-^1 \, S_+$$

$$+ \frac{1}{4} (W4 + i\,W5 + i\,W5 - W7) \, I_-^1 \, S_-$$

$$+\frac{1}{2}\left(W6 - i\,W8\right) I_{+}^{1} S_{z} + \frac{1}{2}\left(W6 + i\,W8\right) I_{-}^{1} S_{z}$$

$$+\frac{1}{2}\left(W6 - i\,W8\right) I_{z}^{1} S_{+} + \frac{1}{2}\left(W6 + i\,W8\right) I_{z}^{1} S_{-}$$

$$+\frac{1}{4}\left(W10 - i\,W11 - i\,W11 - W13\right) I_{+}^{2} S_{+}$$

$$+\frac{1}{4}\left(W10 + i\,W11 - i\,W11 + W13\right) I_{+}^{2} S_{-}$$

$$+\frac{1}{4}\left(W10 - i\,W11 + i\,W11 + W13\right) I_{-}^{2} S_{+}$$

$$+\frac{1}{4}\left(W10 + i\,W11 + i\,W11 - W13\right) I_{-}^{2} S_{-}$$

$$+\frac{1}{2}\left(W12 - i\,W14\right) I_{+}^{2} S_{z} + \frac{1}{2}\left(W12 + i\,W14\right) I_{-}^{2} S_{z}$$

$$+\frac{1}{2}\left(W12 - i\,W14\right) I_{z}^{2} S_{+} + \frac{1}{2}\left(W_{12} + i\,W14\right) I_{z}^{2} S_{-}$$

$$+ W9\, I_{z}^{1} S_{z} + W15\, I_{z}^{2} S_{z} - g_{N}\,\beta_{N}\,H\left(I_{z}^{1} + I_{z}^{2}\right)$$

Defining

$$Q1 = \frac{1}{2}\left(W1 + i\,W2\right)$$

$$Q2 = \frac{1}{4}\left(W4 - W7\right) + \frac{1}{2}\,i\,W5$$

$$Q3 = \frac{1}{4}\left(W4 + W7\right)$$

$$Q4 = \frac{1}{2}\left(W6 + i\,W8\right)$$

$$Q5 = \frac{1}{4}\left(W10 - W13\right) + \frac{1}{2}\,i\,W11$$

$$Q6 = \frac{1}{4}\left(W10 + W13\right)$$

$$Q7 = \frac{1}{2}\left(W12 + i\,W14\right)$$

the spin Hamiltonian becomes

$$H = W3\ S_z + W9\ I_z^1\ S_z + W15\ I_z^2\ S_z - g_N\ \beta_N\ H\ (\ I_z^1 + I_z^2\ )$$

$$+ Q1\ S_- + Q1^*S_+ + Q2^*I_+^1\ S_+ + Q3\ I_+^1\ S_-$$

$$+ Q3\ I_-^1\ S_+ + Q2\ I_-^1\ S_- + Q4^{**}I_+^1\ S_z$$

$$+ Q4\ I_-^1\ S_z + Q4^*I_z^1\ S_+ + Q4\ I_z^1\ S_-$$

$$+ Q5^*I_+^2\ S_+ + Q6\ I_+^2\ S_- + Q6\ I_-^2\ S_+$$

$$+ Q5\ I_-^2\ S_- + Q7^*I_+^2\ S_z + Q7\ I_-^2\ S_z$$

$$+ Q7^*I_z^2\ S_+ + Q7\ I_z^2\ S_-$$

To find the energy eigenvalues of this system, one of the standard methods of quantum mechanics which we use is to set up the Hamiltonian matrix and diagonalize it. The resulting diagonal elements would be the energy eigenstates of the system.

The general form of the Hamiltonian matrix elements can be written as:

$$A(i,j) = \langle M_S, M_{I_1}, M_{I_2} | H | M_S', M_{I_1}', M_{I_2}' \rangle \qquad (3)$$

where M_S (or M_S') is the magnetic quantum number for the electron spin and can have values of $+\frac{1}{2}$ and $-\frac{1}{2}$. M_{I_1} (or M_{I_1}') and M_{I_2} (or M_{I_2}') are the magnetic quantum numbers for the nuclear spins and can have the following values.

$$-I_1 \leq M_{I_1} \leq I_1 \quad \text{and} \quad -I_2 \leq M_{I_2} \leq I_2$$

this gives $2I_1 + 1$ different values for M_{I_1} and $2I_2 + 1$ different values for M_{I_2}, which means the dimension of the resulting Hamiltonian matrix

will be $2(2I_1+1)(2I_2+1)$.

To calculate the matrix elements, we need to use the following well-known relations.

$$S_+ \,|M_S\rangle = \sqrt{(S - M_S)(S + M_S + 1)}\;\; |M_S+1\rangle$$

$$S_- \,|M_S\rangle = \sqrt{(S + M_S)(S - M_S + 1)}\;\; |M_S-1\rangle$$

$$I_+ \,|M_I\rangle = \sqrt{(I - M_I)(I + M_I + 1)}\;\; |M_I+1\rangle$$

$$I_- \,|M_I\rangle = \sqrt{(I + M_I)(I - M_I + 1)}\;\; |M_I-1\rangle$$

Putting these expressions in Equation (3), the nonzero matrix elements can be found.

The set of quantum numbers (M_s, M_{I_1}, M_{I_2}) corresponding to different rows and columns of the Hamiltonian matrix are chosen in the following order.

$(S,I_1,I_2),(S,I_1,I_2-1),.....,(S,I_1,-I_2),(S,I_1-1,I_2),(S,I_1-1,I_2-1),.....,$
$(S,I_1-1,-I_2),.....,(S,-I_1,-I_2),(-S,I_1,I_2),(-S,I_1,I_2-1),....,(-S,I_1,-I_2),(-S,I_1-1,I_2),(-S,I_1-1,I_2-1),.....,(-S,I_1-1,-I_2),.....,(-S,-I_1,-I_2)$

To be more specific if j is the number representing a row or column, j=1 corresponds to the set of quantum numbers (S,I_1,I_2), j=2 corresponds to (S,I_1,I_2-1) and so on.

For the actual calculation of the matrix elements it was noticed that the cases dealing with integer and half-integer values of I_1 and I_2 must be treated separately. Since in this study we will be dealing with half-integer values of I_1 and I_2 it was decided to write the general program for this case.

Let us define the parameters k, i, and t as follows.

$$k = 2I_1+1, \qquad i = 2I_2+1, \qquad t = k.i$$

Since M_{I_1} and M_{I_2} are half-integer values, defining the following integer quantities K_1 and K_2 simplified our programing.

$$K_1 = 2M_{I_1} \quad , \quad K_2 = 2M_{I_2}$$

It was found that by writing K_1 and K_2 in terms of integer quantities 1 and m and then generating all possible pairs (1,m), one can generate all possible values of K_1 and K_2.

It will be seen later that each nonzero matrix element can be identified by a simple index(j) and some constants. To generate each matrix element in such a way that its index (j) be correlated with the corresponding K_1 and K_2, we wrote the following expressions for K_1, K_2 and j in terms of 1 and m.

$$j = 1.m + (1-1)(i-m)$$

$$K_1 = k + 1 - 21$$

$$K_2 = i + 1 - 2m$$

Then we chose all possible values of the pair (1,m) in the limit of $1 \leq 1 \leq k$, $1 \leq m \leq i$ and used each pair to determine j, K_1, K_2, and the corresponding matrix element.

The following is the list of the different <u>groups</u> of matrix elements.

$$A(j,j) = \tfrac{1}{2}\, W3 + \tfrac{1}{4}\, K_1\, W9 + \tfrac{1}{4}\, K_2\, W15 - \tfrac{1}{2}\, g_N\, \beta_N\, H\, (K_1 + K_2)$$

$$A(j+t,j+t) = -\tfrac{1}{2}\, W3 - \tfrac{1}{4}\, K_1 W9 - \tfrac{1}{4}\, K_2\, W15 - \tfrac{1}{2}\, g_N\, \beta_N\, H\, (K_1 + K_2)$$

$$A(j+t,j) = Q1 + \tfrac{1}{2} K_1 \, Q4 + \tfrac{1}{2} K_2 \, Q7$$

In the next three expressions, simultaneous values of l=k and m=i must be excluded.

$$A(j+1,j) = \tfrac{1}{2} Q7 \sqrt{(I_2 + \tfrac{1}{2} K_2)(I_2 - \tfrac{1}{2} K_2 + 1)}$$

$$A(j+t+1,j+t) = - A(j+1,j)$$

$$A(j+t+1,j) = Q5 \sqrt{(I_2 + \tfrac{1}{2} K_2)(I_2 - \tfrac{1}{2} K_2 + 1)}$$

In the following five expressions, the series of matrix elements corresponding to l=k must be excluded.

$$A(j+i,j) = \tfrac{1}{2} Q4 \sqrt{(I_1 + \tfrac{1}{2} K_1)(I_1 - \tfrac{1}{2} K_1 + 1)}$$

$$A(j+i+t,j+t) = - A(j+i,j)$$

$$A(j+i+t,j) = Q2 \sqrt{(I_1 + \tfrac{1}{2} K_1)(I_1 - \tfrac{1}{2} K_1 + 1)}$$

$$A(m+t,m+1) = Q6 \sqrt{(I_2 - \tfrac{1}{2} K_2 + 1)(I_2 + \tfrac{1}{2} K_2)}$$

$$A(m+t+1.i,m+1+1.i) = A(m+t,m+1)$$

For the case of $I_1 = I_2 = \tfrac{1}{2}$ the following elements should be added.

$$A(5,3) = A(6,4) = Q3$$

Since the spin Hamiltonian matrix is Hermitian, it must be symmetric and only matrix elements of the lower triangle are needed. By diagonalizing this Hamiltonian matrix the energy eigenvalues of the system can be obtained. For the H and H_A centers in $RbCaF_3$, the two nuclei are fluorine with $I_1 = I_2 = \tfrac{1}{2}$. Therefore, the Hamiltonian matrix will be

8 X 8 as shown in Table I. The diagonalization of this matrix gives eight energy levels. Considering the selection rule for ESR, $\Delta M_S = \pm 1$, $\Delta M_I = 0$, we obtain four possible transitions. Experimentally, a suitable microwave frequency (approximately 9.2 Ghz) is chosen (33) and the magnetic field is varied until a resonance (i.e., an absorption of microwave power) is obtained. Therefore the different transitions are identified by their corresponding values of the magnetic field.

Two computer programs were written which are listed in Appendixes A and B. The first program (Appendix A) assumes that the spin Hamiltonian parameters are known and computes the line positions as a function of magnetic field direction. This is accomplished by an iteration process in which the magnetic field magnitude is varied until the calculated transition frequency corresponds to the experimental microwave frequency. In the second program (Appendix B), an initial set of spin Hamiltonian parameters and the experimental line positions are given. For the given Hamiltonian parameters, the transition frequencies corresponding to each of the experimental line positions (i.e., magnetic field values) are calculated and compared to the experimental microwave frequency. Then the process is repeated as the Hamiltonian parameters are systematically varied until all of the calculated frequencies agree with the experimental microwave frequency (within the experimental error). These final parameters are then used in the first program to find the best calculated line positions. These two programs are set up in such a way that can be used for any case of half-integer spin nuclei.

TABLE I

LOWER HALF OF THE HAMILTONIAN MATRIX FOR H AND H_A CENTERS IN $RbCaF_3$

	$\lvert +\frac{1}{2}, +\frac{1}{2}, +\frac{1}{2}\rangle$	$\lvert +\frac{1}{2}, +\frac{1}{2}, -\frac{1}{2}\rangle$	$\lvert +\frac{1}{2}, -\frac{1}{2}, +\frac{1}{2}\rangle$	$\lvert +\frac{1}{2}, -\frac{1}{2}, -\frac{1}{2}\rangle$	$\lvert -\frac{1}{2}, +\frac{1}{2}, +\frac{1}{2}\rangle$	$\lvert -\frac{1}{2}, +\frac{1}{2}, -\frac{1}{2}\rangle$	$\lvert -\frac{1}{2}, -\frac{1}{2}, +\frac{1}{2}\rangle$	$\lvert -\frac{1}{2}, -\frac{1}{2}, -\frac{1}{2}\rangle$
$\langle +\frac{1}{2}, +\frac{1}{2}, +\frac{1}{2}\rvert$	A(1,1)							
$\langle +\frac{1}{2}, +\frac{1}{2}, -\frac{1}{2}\rvert$	A(2,1)	A(2,2)						
$\langle +\frac{1}{2}, -\frac{1}{2}, +\frac{1}{2}\rvert$	A(3,1)	0	A(3,3)					
$\langle +\frac{1}{2}, -\frac{1}{2}, -\frac{1}{2}\rvert$	0	A(4,2)	A(4,3)	A(4,4)				
$\langle -\frac{1}{2}, +\frac{1}{2}, +\frac{1}{2}\rvert$	A(5,1)	A(5,2)	A(5,3)	0	A(5,5)			
$\langle -\frac{1}{2}, +\frac{1}{2}, -\frac{1}{2}\rvert$	A(6,1)	A(6,2)	0	A(6,4)	A(6,5)	A(6,6)		
$\langle -\frac{1}{2}, -\frac{1}{2}, +\frac{1}{2}\rvert$	A(7,1)	0	A(7,3)	A(7,4)	A(7,5)	0	A(7,7)	
$\langle -\frac{1}{2}, -\frac{1}{2}, -\frac{1}{2}\rvert$	0	A(8,2)	A(8,3)	A(8,4)	0	A(8,6)	A(8,7)	A(8,8)

CHAPTER III

EXPERIMENTAL PROCEDURE

Sample Preparation

The $RbCaF_3$ crystals used in this study were obtained from Dr. E. Sonder of the Oak Ridge National Laboratories and are from the same batch as those used by Modine, Sonder, and Unruh (26). These crystals were prepared by a Bridgeman technique from high-purity powders of RbF and CaF_2, both greater than 99.9% purity. According to Modine et al (26),

> The mixtures were inserted in conical-bottomed platinum ampoules (2-cm diameter X 6 cm X 0.5-mm wall thickness), which were then welded shut under a roughing pump vacuum. The charged ampoules were heated to approximately 50° above the melting point of $RbCaF_3$ (1110°C) and subsequently lowered to room temperature through a temperature gradient of 20°C/cm at rates of 1 to 3 mm/h. In a variation of the technique, unsealed high-density graphite containers were used under 2-atm pressure of either pure argon or helium containing 5% hydrogen by volume. The crystals contained a number of impurities which came primarily from the starting materials. The predominent contaminants of one ingot are listed in Table II (p. 1623).

Defect Production

The production of defects in $RbCaF_3$ was carried out by electron irradiation using a Van de Graaff accelerator. The irradiations were done with 1.5 Mev electrons and 10 μA total current (0.2 μA on the sample). The sample was placed in a styrofoam cup containing liquid nitrogen with its broad side against the cup wall. The cup was placed a distance of 5 cm in front of the accelerator window. The styrofoam cup and the

TABLE II

MAJOR IMPURITIES IN $RbCaF_3$ CRYSTALS AS OBTAINED FROM SPARK SPECTRA ANALYSIS. (FROM REFERENCE 26)

	Approximate Concentration (ppm)
Al	100
Fe	10
K	1000
Mg	20
Na	100
Cs	100

liquid nitrogen were changed after every five minutes of irradiation to prevent any possible explosion due to irradiation of liquid nitrogen.

ESR Spectrometer

The spectrometer used in this study was an X-band homodyne type which is shown in Figure 4. It is composed of a microwave bridge, magnet system, and modulation and detection systems. The microwave bridge includes the components which control, or measure, the frequency and intensity of the microwave beam and direct the microwave beam to and from the sample. The source of microwave radiation is a klystron, i.e., a vacuum tube producing microwave oscillations centered on a small range of frequencies. In practice the klystron will be locked to the resonant frequency of the cavity by using a frequency stablizer. An isolator is used which prevents any backward reflection of microwave energy to the klystron. The attenuator adjusts the amount of microwave power incident on the sample which is placed inside the microwave cavity. The circulator is a nonreciprocal three-port device which passes the wave traveling in the forward direction but strongly attenuates the one traveling in the other direction. It is used to direct microwave power to the cavity and to direct the signal reflected from the cavity to the detector. A terminating load absorbs any power which might be reflected from the detector arm.

The magnet system provides a stable, variable, and homogeneous magnetic field and consists of a 9-inch Varian V-7200 electromagnet. Stability of the field is achieved by the use of a Hall probe mounted on one of the caps. It can detect any variations in the field intensity and adjust the magnet current by supplying an error signal.

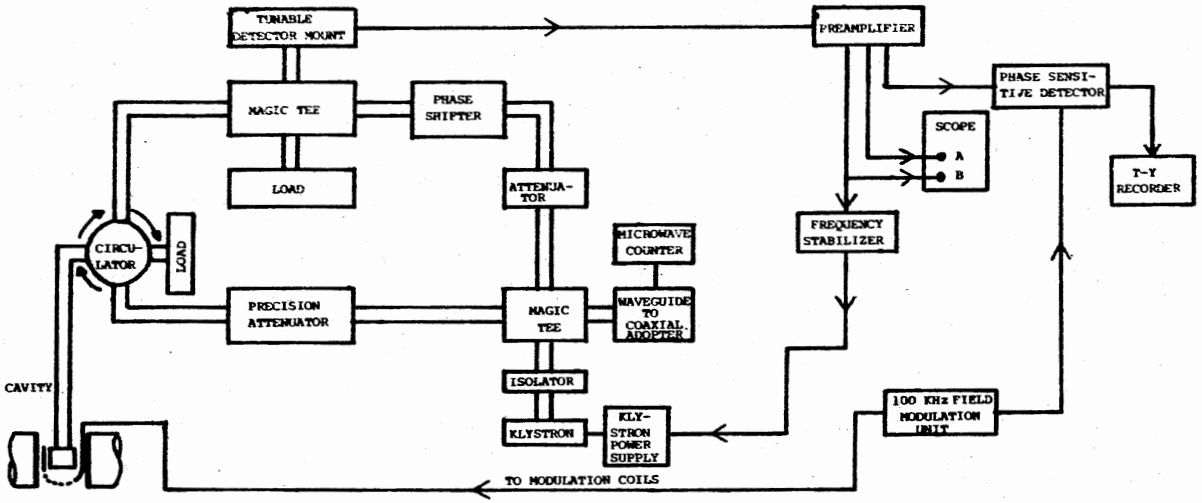

Figure 4. ESR Spectrometer

The modulation and detection systems monitor, amplify, and record the ESR signal. The modulation of the magnetic field was done by a 100 kHz modulation unit. The modulation coils were built into the Varian 4531 cavity. The microwave signal was detected using a properly biased low-noise Schottky barrier diode. This signal was then amplified by a broad-band amplifier and fed to a phase sensitive detector which greatly enhaced the signal-to-noise ratio. The reference signal for the phase sensitive detector was obtained from the same oscillator as used to amplitude modulate the static magnetic field. The output of the phase sensitive detector was fed onto a chart recorder.

The sample was loaded in the sample holder shown in Figure 5. Its upper part of the tube is stainless steel and the lower part is teflon which holds the sample. The center rod was then pushed down by a spring to hold the sample in position. The sample was then lowered into a finger Dewar filled with liquid nitrogen and the finger Dewar was then placed in the microwave cavity.

Ultraviolet Bleaching

In our study it was necessary to remove parts of the ESR spectra due to different defects. This was done with the use of a 100 watt mercury lamp. The beam of the lamp was focused on the sample through a window in the cavity.

Thermal Anneal Studies

Thermal anneal studies were achieved by the use of a Varian variable temperature accessory. The system operated on the basis of heat exchange between nitrogen gas and liquid nitrogen. The temperature of the gas

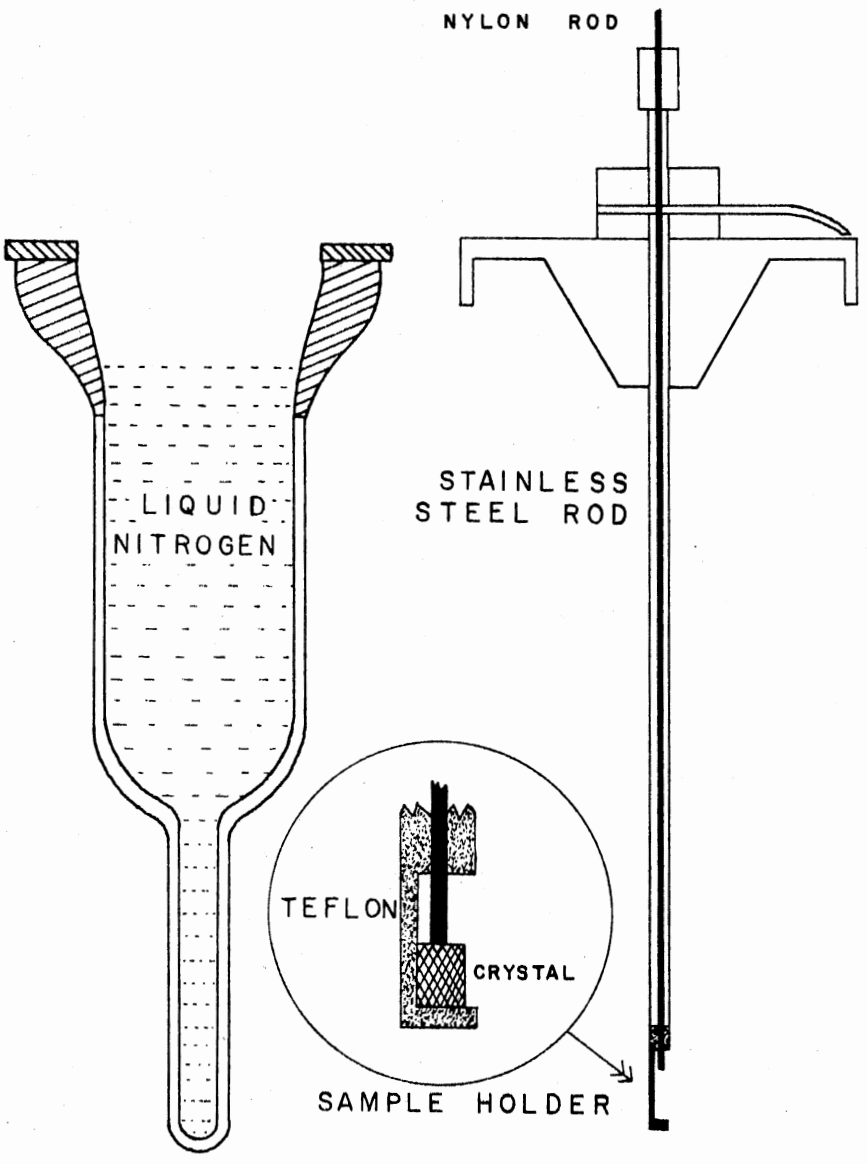

Figure 5. Sample Holder and Finger Dewar Used in ESR Measurements

could be changed by varying the rate of flow through the heat exchanger and also by heater element placed in the gas stream. The temperatures were monitored by a copper vs. constantan thermocouple. In the anneal studies, the sample was held at a fixed temperature for three minutes before returning to the base temperature and recording the ESR spectra.

Magnetic Field Measurement

The measurement of the magnetic field was accomplished through the use of an NMR proton probe. The source of the protons was glycerine. In practice, the NMR resonance frequencies corresponding to each line were measured and converted to magnetic field by the use of the following relationship (2):

$$H \text{ (in gauss)} = 234.87 \, \nu_p \text{ (in MHS)}$$

Since the sample position and the probe position were not quite the same, the measured magnetic field had to be corrected. This correction was obtained from an $MgO:Cr^{3+}$ sample (Cr^{3+} g value equals 1.9799) and assumed to vary linearly with the magnetic field.

CHAPTER IV

EXPERIMENTAL RESULTS

As was mentioned in Chapter I, when a $RbCaF_3$ crystal is taken to temperatures below 196 K, a twisting of the CaF_6 octahedra about the tetragonal axis is observed. This axis will be referred to as the z, or [001] axis. Figure 6 shows the 77 K spectrum when the magnetic field is along the [001] axis. The line assignments are shown by the stick diagram in Figure 6. The lines assigned to the $[F_2^-]$ center have been analyzed by Halliburton and Sonder (29). The three 0° lines assigned to the H center have intensity ratios of 1:2:1. A theoretical model for this kind of spectrum must consist of two equivalent spin ½ nuclei (33) This leads to the conclusion that the nuclear hyperfine tensors must be the same ($\overleftrightarrow{A}_1 = \overleftrightarrow{A}_2$). The two nuclei involved can be assumed to be fluorines, because their nuclear spin is ½ and that of the other constituents of the crystal is not.

To observe the H center spectrum more clearly, the $[F_2^-]$ center spectrum was eliminated by bleaching the sample with ultraviolet light. The remaining spectrum is due to H center and is shown in Figure 6d. It exhibits three small lines on the low field side of the large central line. These three lines plus a fourth line underlying the central line are due to the H centers aligned perpendicular to the magnetic field. From this result it can be concluded that the x and y components of the principal axes of the $\overleftrightarrow{g}$ and $\overleftrightarrow{A}$ tensors must be equivalent. If that were

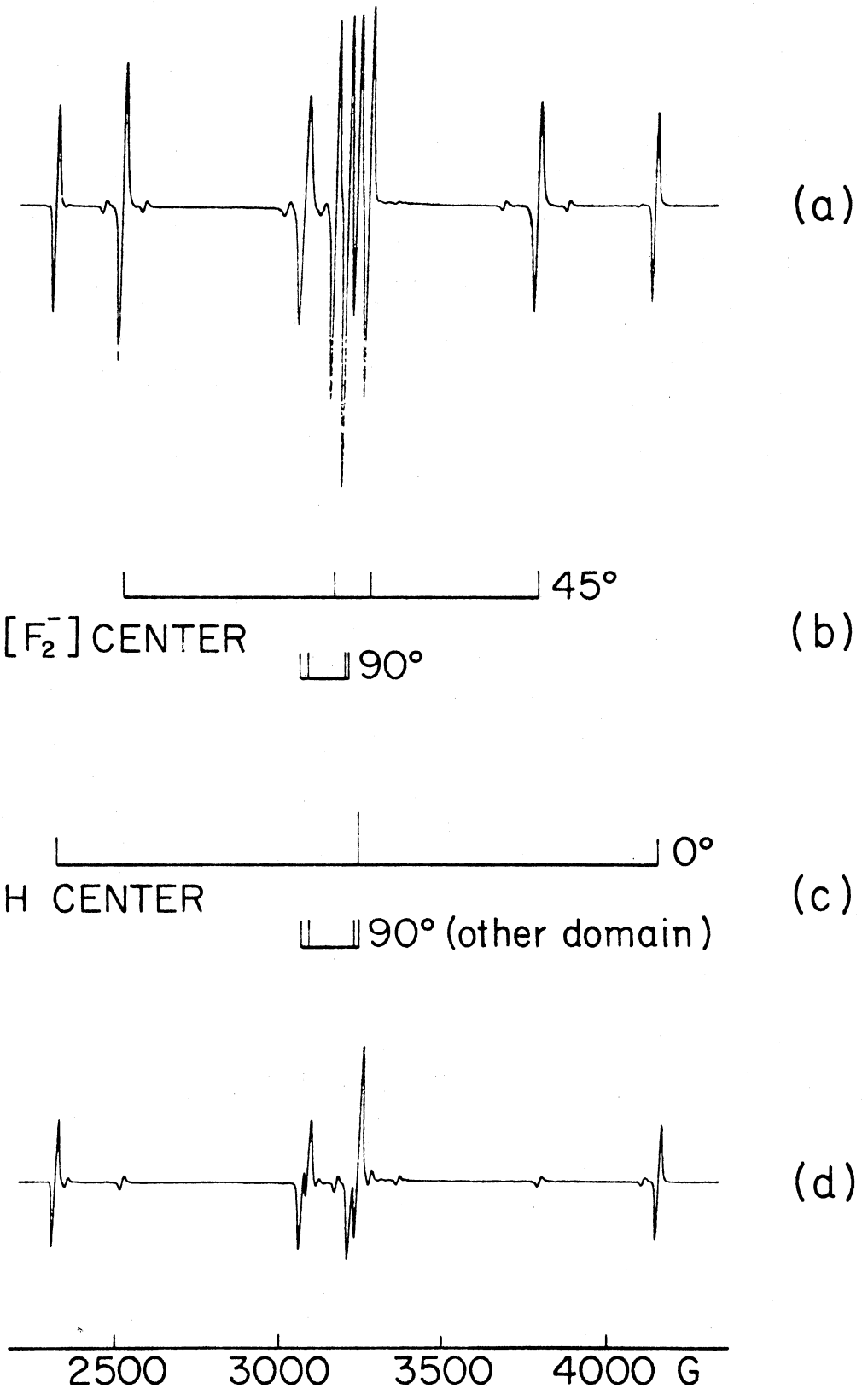

Figure 6. [001] Spectrum of $[F_2^-]$ and H Center in $RbCaF_3$ at 77 K

not so, we would get a second set of similar lines near the center of the spectrum because of the two inequivalent ways the magnetic field can be oriented (parallel to x or y) perpendicular to the molecular axis of the H centers.

A production study of defects in $RbCaF_3$ gives us much additional information. The results of this production study are given in Figure 7. The $[F_2^-]$ centers grow and saturate very fast while the spectra assumed to be due to H center grows much slower. This means that the radiation-induced defect labeled H center is an ionic defect (i.e., requires motion of ions during formation) compared to the $[F_2^-]$ center which is an electronic defect (only requires rearrangement of the electrons and holes). Therefore, assuming the H center is a radiation-induced interstitial fluorine is correct.

Considering these charactristics, the model for the H center can be pictured as in Figure 8. Figure 9 shows the six different possible orientations for the centers (A, B, C, D, E, F) belonging to the three possible domains. Since there is no evidence to the contrary, it was assumed that the principal axis (z) of each of the $\overleftrightarrow{g}$ and $\overleftrightarrow{A}$ tensors should be coaxial with the [001] crystal axis. Therefore the three different transformation matrices defined in Chapter II can be redefined as:

$$[TG] = [T1] = [T2] \equiv [T]$$

Choosing the z-axis for the transformation matrices along the arrows in Figure 9 and the x-axis pointing in toward the calcium ion, the transformation matrices corresponding to the six centers can be written as the following:

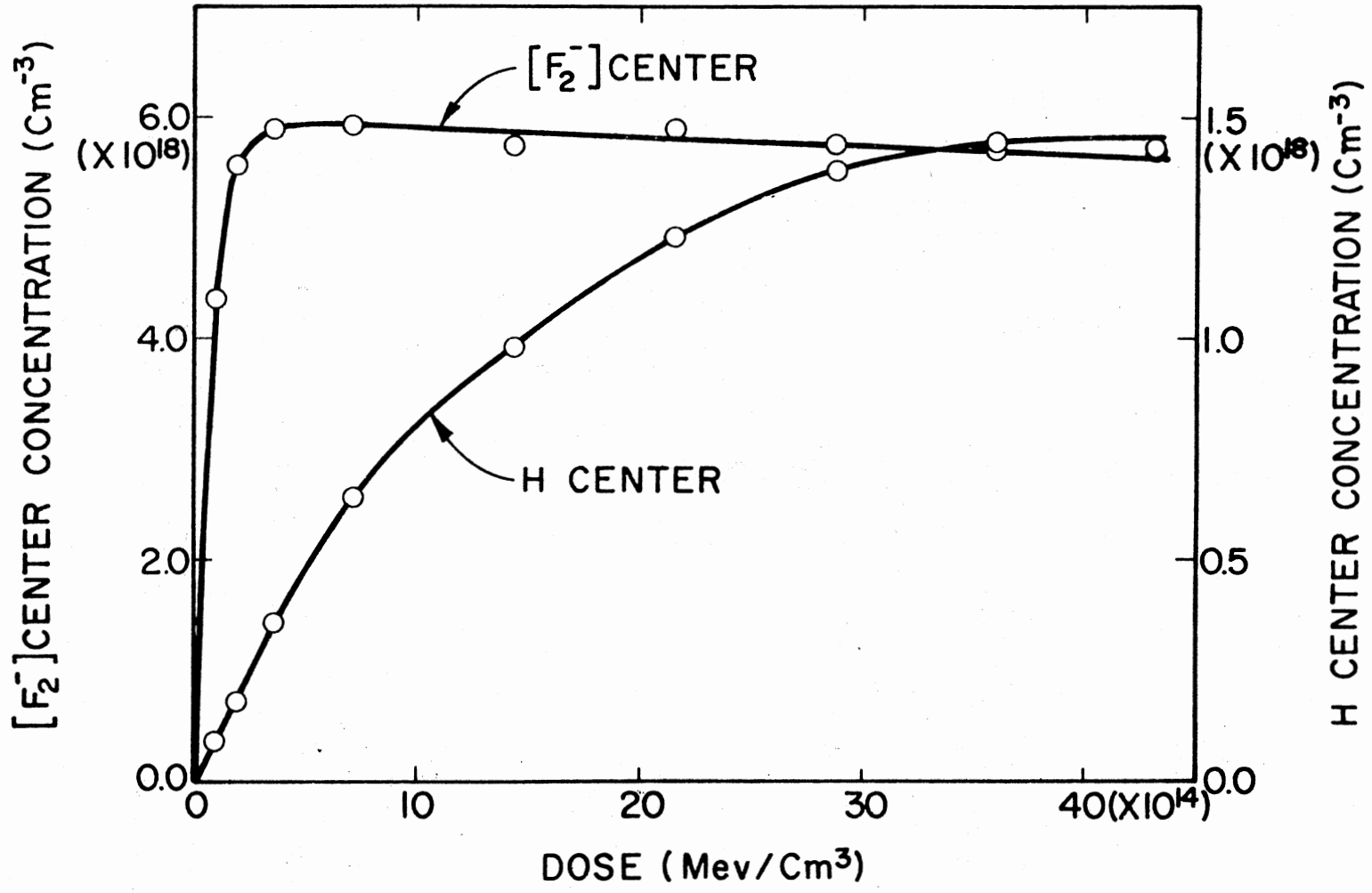

Figure 7. Production Study of $[F_2^-]$ and H Centers in $RbCaF_3$

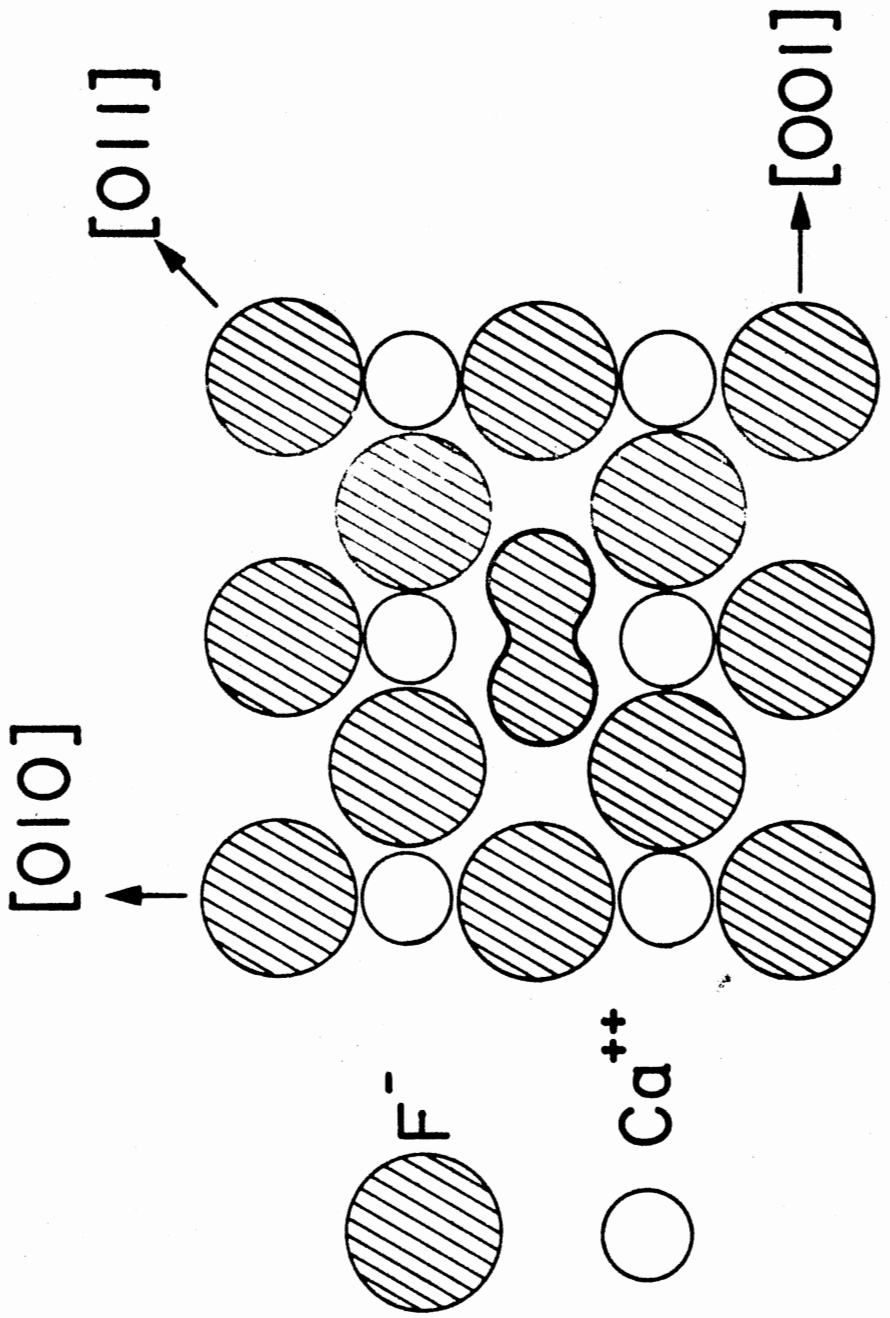

Figure 8. Model for the H Center in $RbCaF_3$

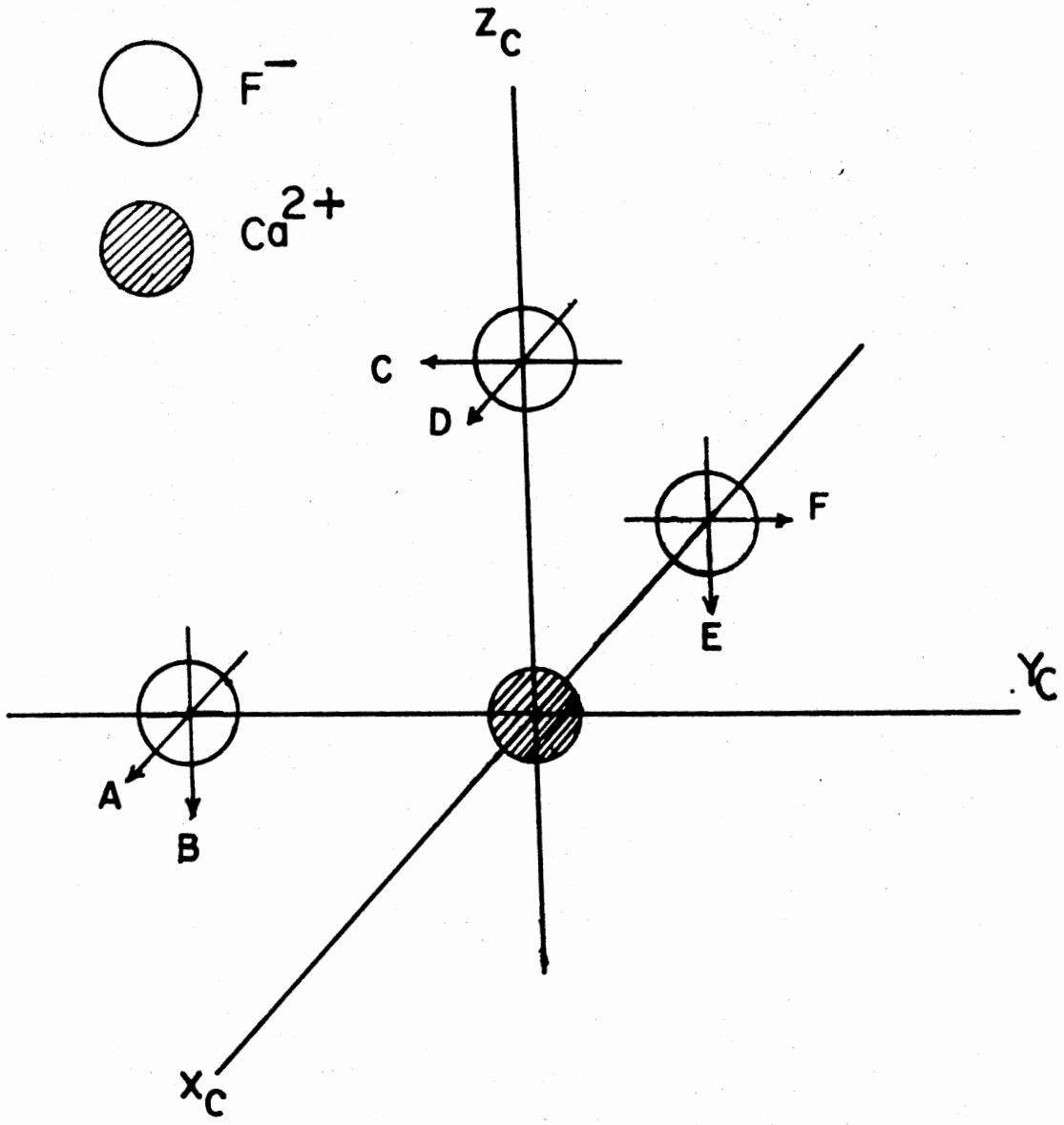

Figure 9. Six Different Possible Orientations for the H Center in $RbCaF_3$

$$[T]_A = \begin{pmatrix} 0 & 1 & 0 \\ 0 & 0 & 1 \\ 1 & 0 & 0 \end{pmatrix} \qquad [T]_B = \begin{pmatrix} 0 & 1 & 0 \\ 1 & 0 & 0 \\ 0 & 0 & -1 \end{pmatrix}$$

$$[T]_C = \begin{pmatrix} 0 & 0 & -1 \\ 1 & 0 & 0 \\ 0 & -1 & 0 \end{pmatrix} \qquad [T]_D = \begin{pmatrix} 0 & 0 & -1 \\ 0 & 1 & 0 \\ 1 & 0 & 0 \end{pmatrix}$$

$$[T]_E = \begin{pmatrix} 1 & 0 & 0 \\ 0 & -1 & 0 \\ 0 & 0 & -1 \end{pmatrix} \qquad [T]_F = \begin{pmatrix} 1 & 0 & 0 \\ 0 & 0 & -1 \\ 0 & 1 & 0 \end{pmatrix}$$

With the help of Figure 10, the transformation matrix [R] which transforms the crystal coordinate system to the magnetic coordinate system, can be written as:

$$[R] = \begin{pmatrix} \cos\theta & -\sin\theta\ \sin\phi & \sin\theta\ \cos\phi \\ 0 & \cos\phi & \sin\phi \\ -\sin\theta & -\cos\theta\ \sin\phi & \cos\theta\ \cos\phi \end{pmatrix}$$

Using one of the computer programs described in Chapter II, the spin Hamiltonian parameters were calculated to fit the measured line positions given in Table III. The resulting parameters are given in Table IV.

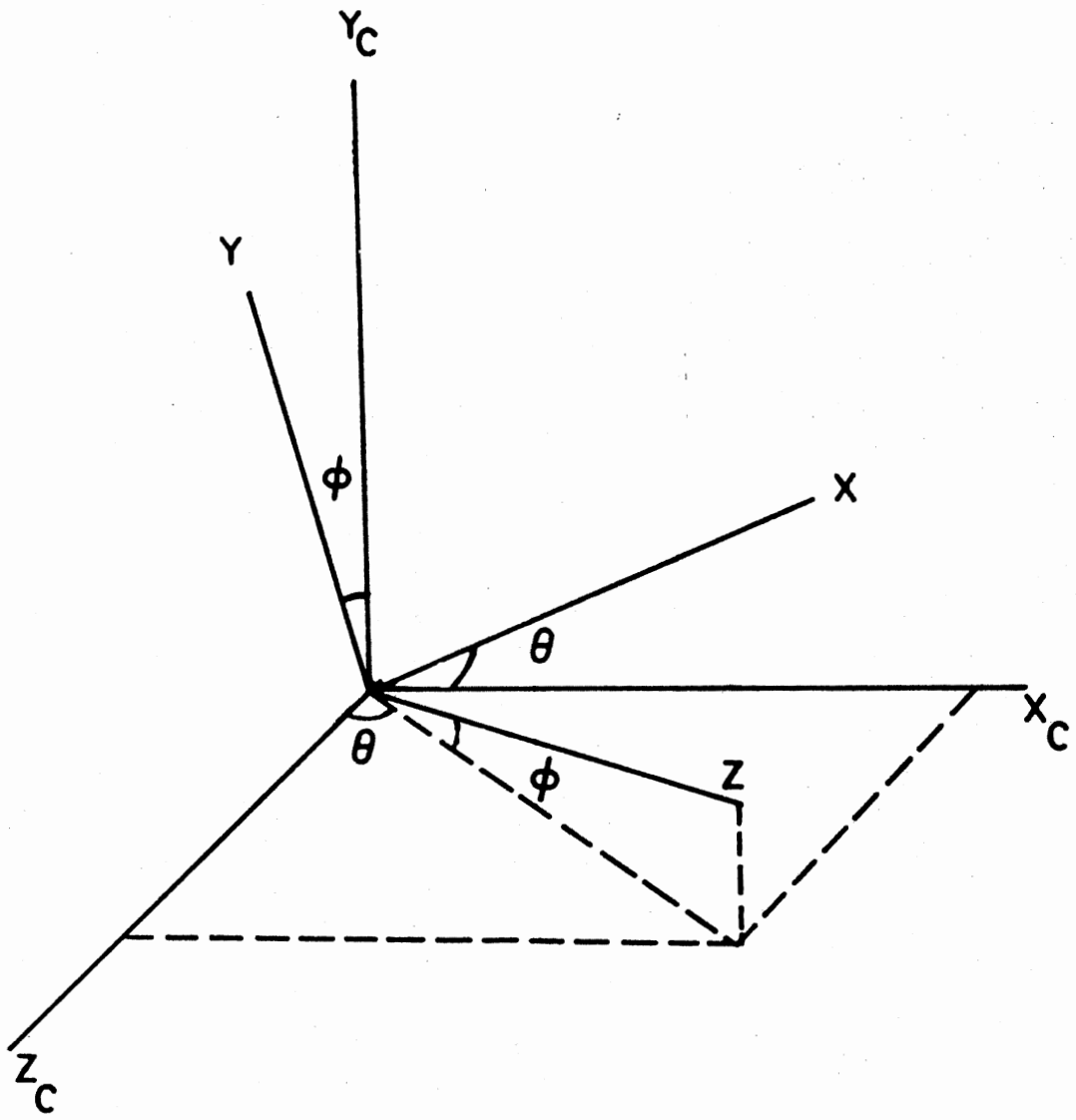

Figure 10. The Crystal Coordinate and the Magnetic Coordinate Systems

TABLE III

CALCULATED AND MEASURED LINE POSITIONS (IN GAUSS) OF THE H CENTER FOR THE 001 DIRECTION

Experimental	Calculated
2327.33	2327.22
3080.58	3080.52
3095.12	3097.64
3232.86	3230.64
3246.29*	3247.49
	3248.04
	3248.39
4168.80	4169.31

Microwave frequency = 9.09967 GHz

* Not used in analysis.

TABLE IV

SPIN HAMILTONIAN PARAMETERS OF THE H CENTER IN $RbCaF_3$

$g_x = g_y$	2.0133 ± 0.0005
g_z	2.0023 ± 0.0003
$A_x = A_y$	138 ± 10 MHz
A_z	2580 ± 10 MHz

The thermal annealing of the $[F_2^-]$ and H centers was done and the results are shown in Figure 11. As can be seen, the $[F_2^-]$ and H centers decay between 110 K and 150 K. At about 110 K, a new set of lines appeared. These new lines grew until 150 K and then started to decay. This new center has been tentatively called an H_A center.

Now the question becomes whether the precursor of this new spectrum is the H center or the $[F_2^-]$ center. To answer this question, two sets of thermal anneal experiments were done. In one the sample was irradiated for 10 seconds and in the other one the irradiation time was 10 minutes. As illustrated in Figure 7, the intensities of the $[F_2^-]$ centers are very similar for both the short and long irradiations while the intensities of the H center are quite different (lower for the 10 second irradiation time and higher for the 10 minute irradiation time). It was observed that the maximum intensities of the H_A center lines (which are obtained upon anneal to 150 K) following the two different irradiation times corresponds to the intensity of the initial H center lines (i.e., lower for the 10 second irradiation time and higher for the 10 minute irradiation time). Therefore, the H_A center appears to originate in the H center.

One of the goals in this study was to characterize the H_A center. In order to do this, the sample was first irradiated at 77 K for about 10 minutes and then warmed up to 150 K to form H_A centers. The resulting H_A centers were observed at 77 K. The [001] spectrum of the H_A center at 77 K is shown in Figure 12. It consists of four equally intense lines. Therefore, all possible orientations of the center with respect to the [001] direction must be equivalent. Figure 13 shows all the possible orientations of the H_A center which are consistent with the [001] spect-

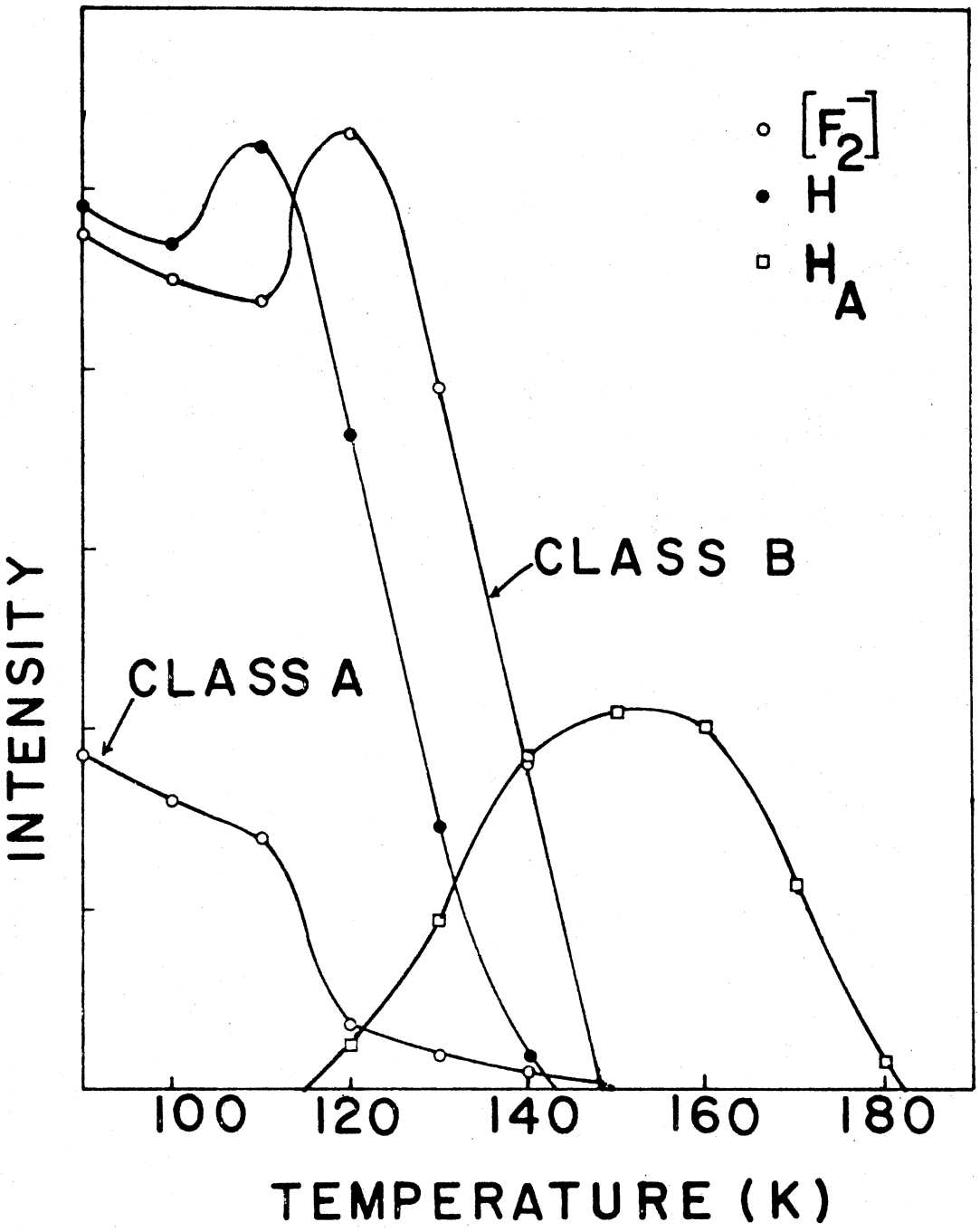

Figure 11. Thermal Annealing of the $[F_2^-]$ and H Centers in $RbCaF_3$ (For Definition of the Two Classes see Reference 29)

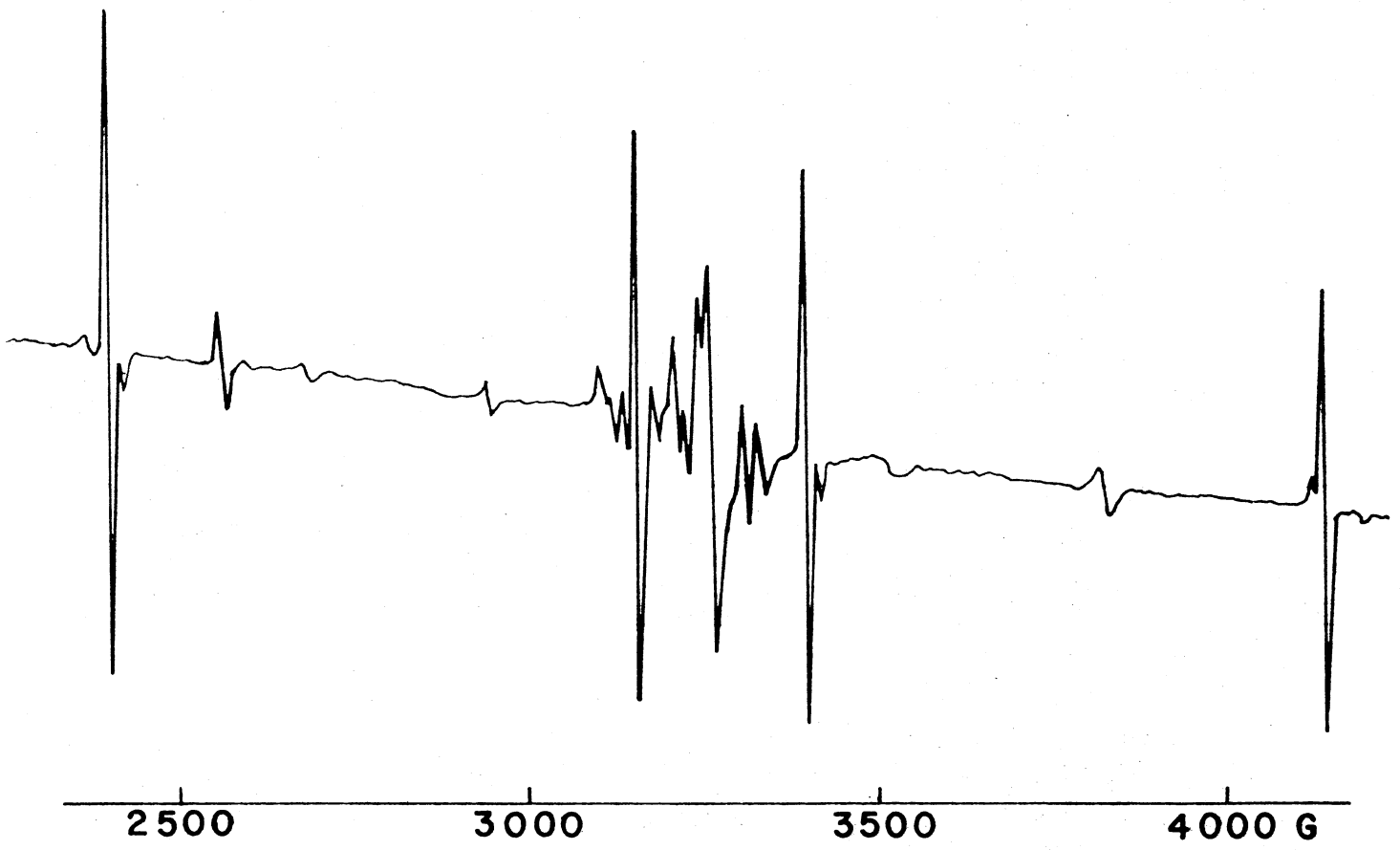

Figure 12. [001] Spectrum of the H_A Center in $RbCaF_3$ at 77 K

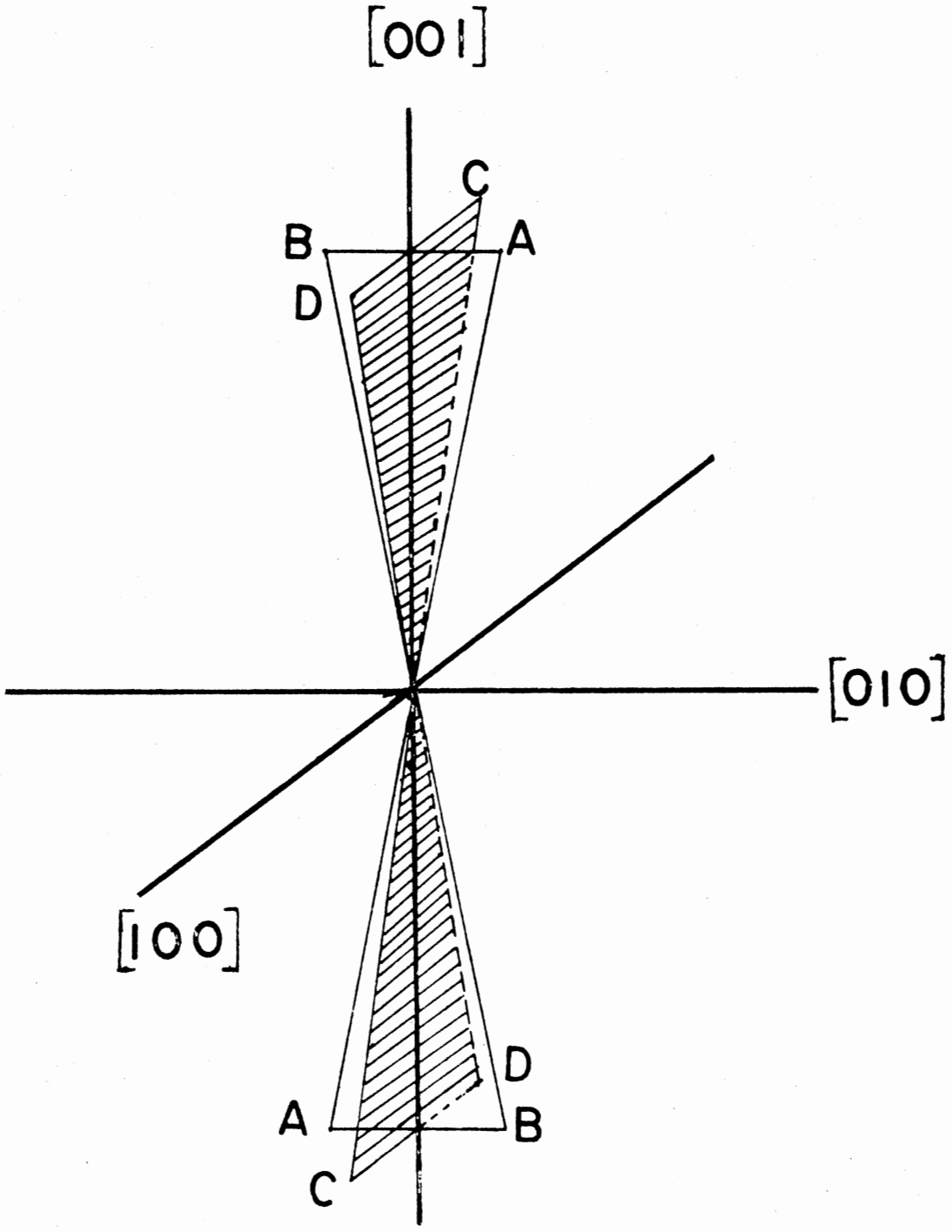

Figure 13. Possible Orientations of the H_A Center in $RbCaF_3$

rum and the other spectra which will be discussed later. The [101] spectrum which is shown in Figure 14 consists of three sets of lines, each set consisting of four lines. The orientation designations A, B, C, and D are shown in Figure 13 and the lines corresponding to each orientation are shown by the stick diagram below the spectrum in Figure 14. In the [101] spectrum, orientations A and B are equivalent and we get a doubly intense set of lines compared to the orientations C or D. The [100] spectrum of the H_A centers in $RbCaF_3$ at 77 K is shown in Figure 15. For this direction of the magnetic field the A and B as well as C and D orientations are pairwise equivalent. This fact is apparent from the stick diagram in Figure 15.

The computer-generated angular behavior of the H_A center in $RbCaF_3$ is given in Figure 16. Figure 17 shows the model for H_A center in $RbCaF_3$.

To find the transformation matrices defined in Chapter II for the four different orientations, we chose the y_i axis of a given tensor to be toward the calcium neighbor of a fluorine site, and the z_i axis to be along the axis connecting the two fluorine atoms. Figure 18 shows the schematic representation and orientations of the three principal axes coordinate systems pertinent to the $\overleftrightarrow{g}$, $\overleftrightarrow{A}_1$, and $\overleftrightarrow{A}_2$ tensors.

The resulting transformation matrices for the four different possible orientations are as follows.

For site A

$$[T]_i = \begin{pmatrix} 0 & -\cos\theta_i & \sin\theta_i \\ 1 & 0 & 0 \\ 0 & \sin\theta_i & \cos\theta_i \end{pmatrix}$$

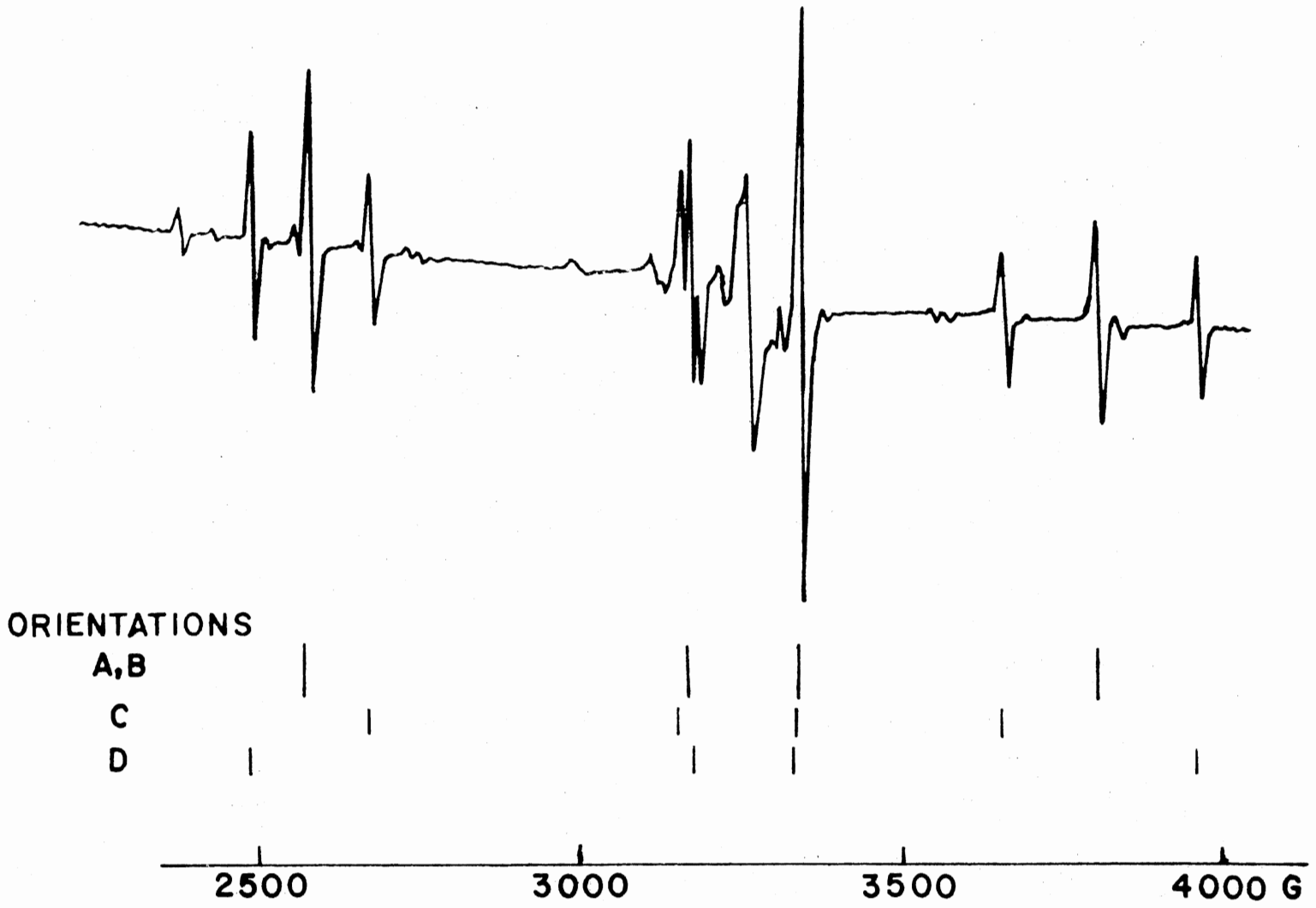

Figure 14. [101] Spectrum of the H_A Center in $RbCaF_3$ at 77 K

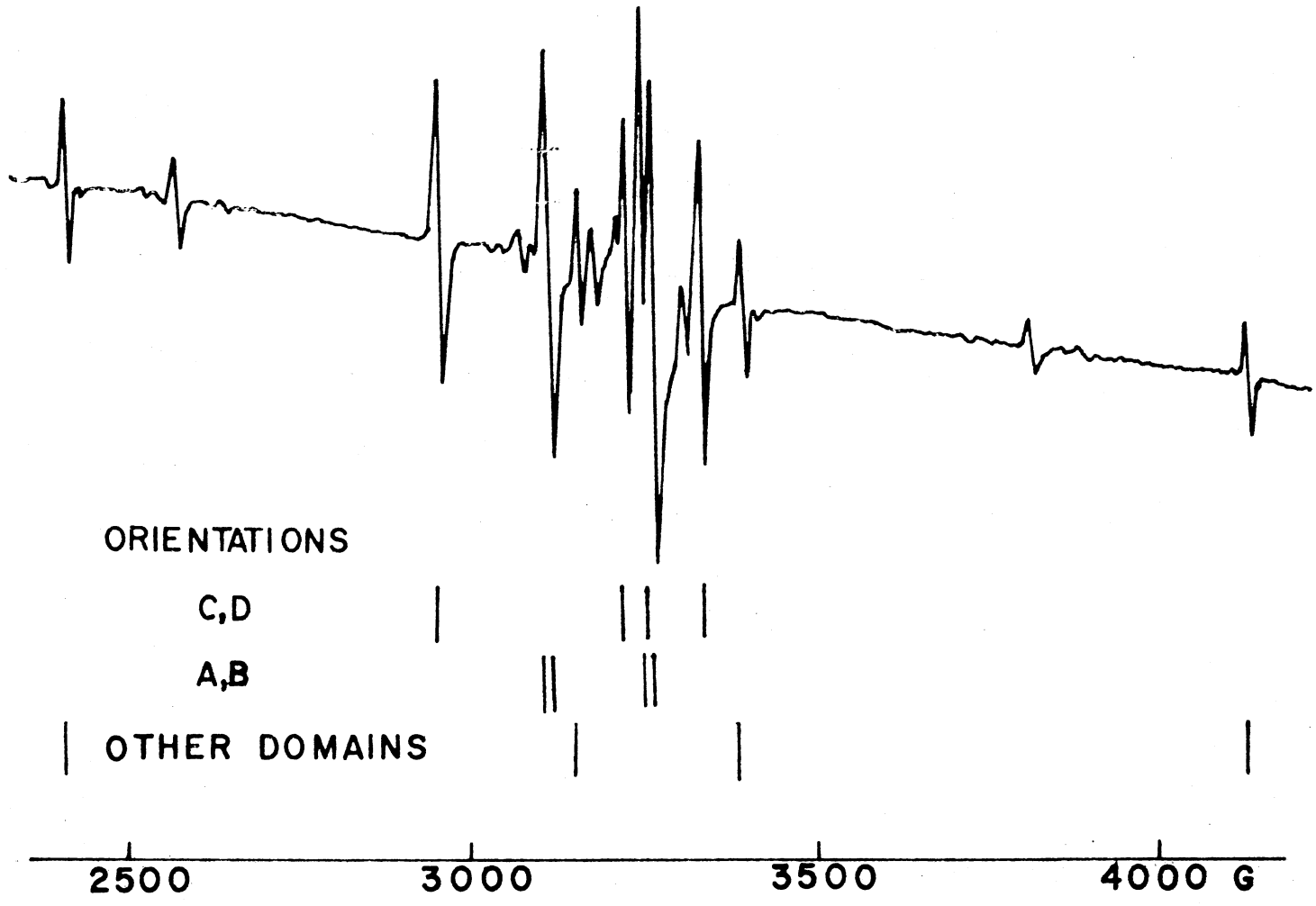

Figure 15. [100] Spectrum of the H_A Center in $RbCaF_3$ at 77 K

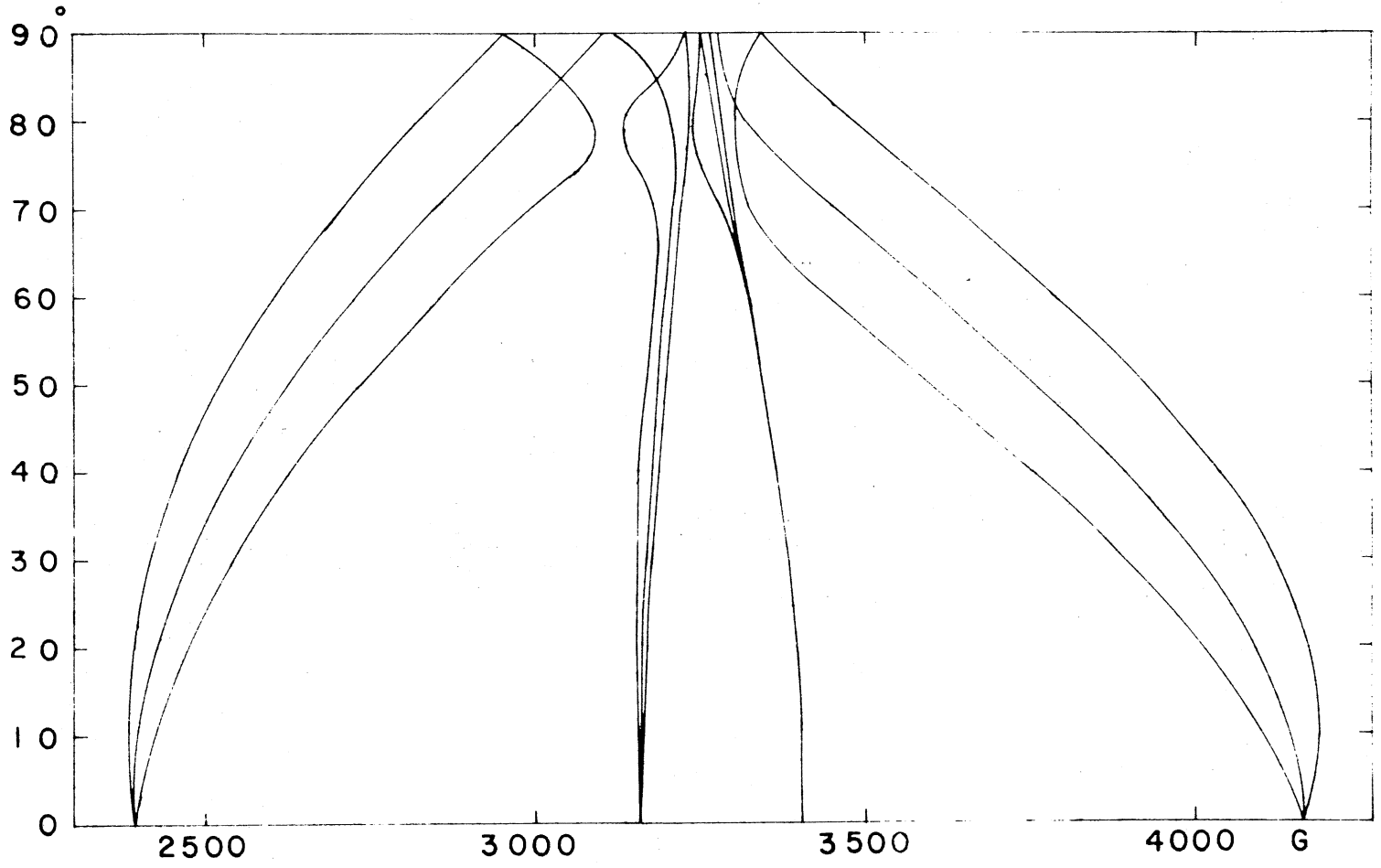

Figure 16. Computer-Generated Angular Behavior of the H_A Center in $RbCaF_3$

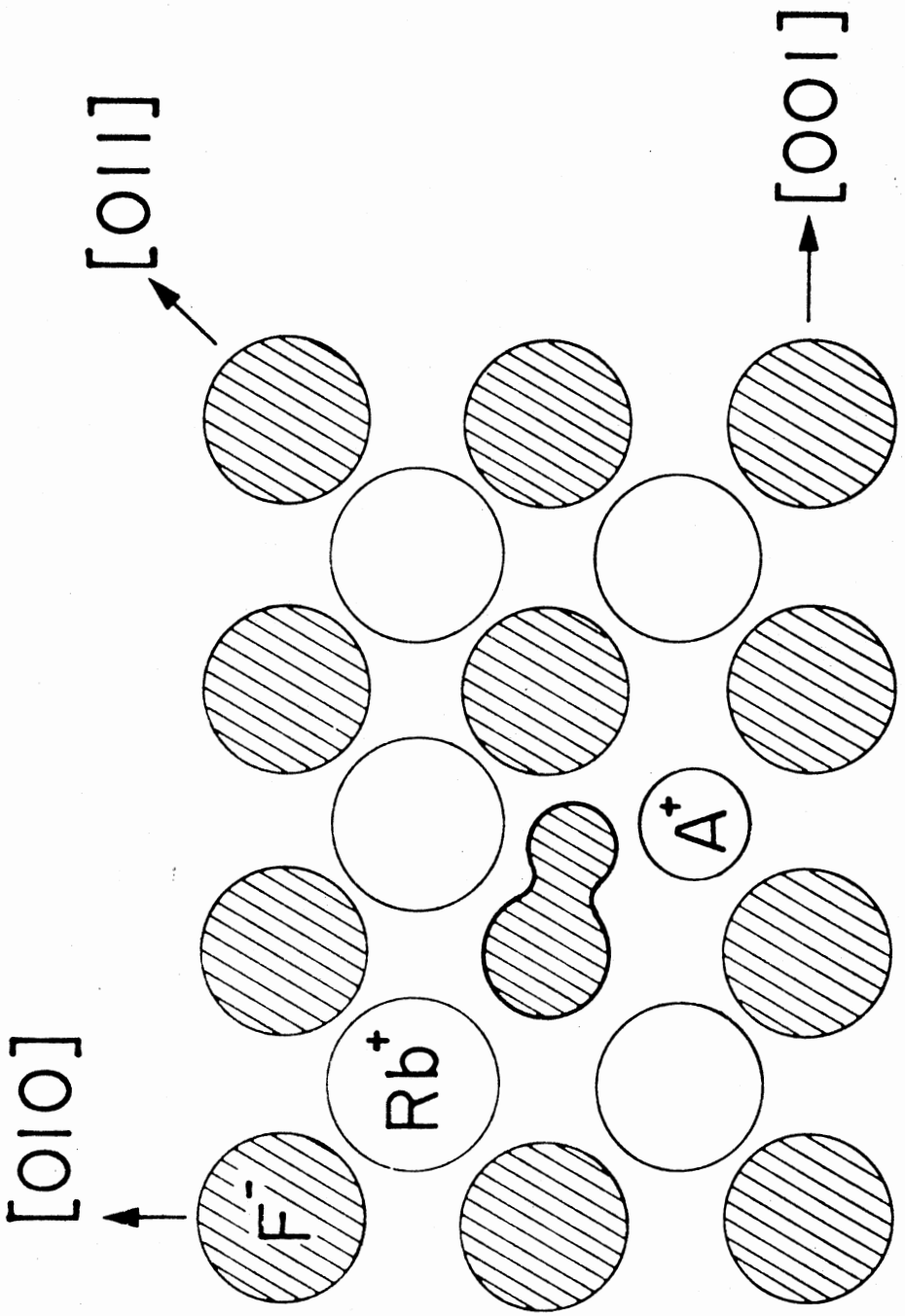

Figure 17. Model for H_A Center in $RbCaF_3$

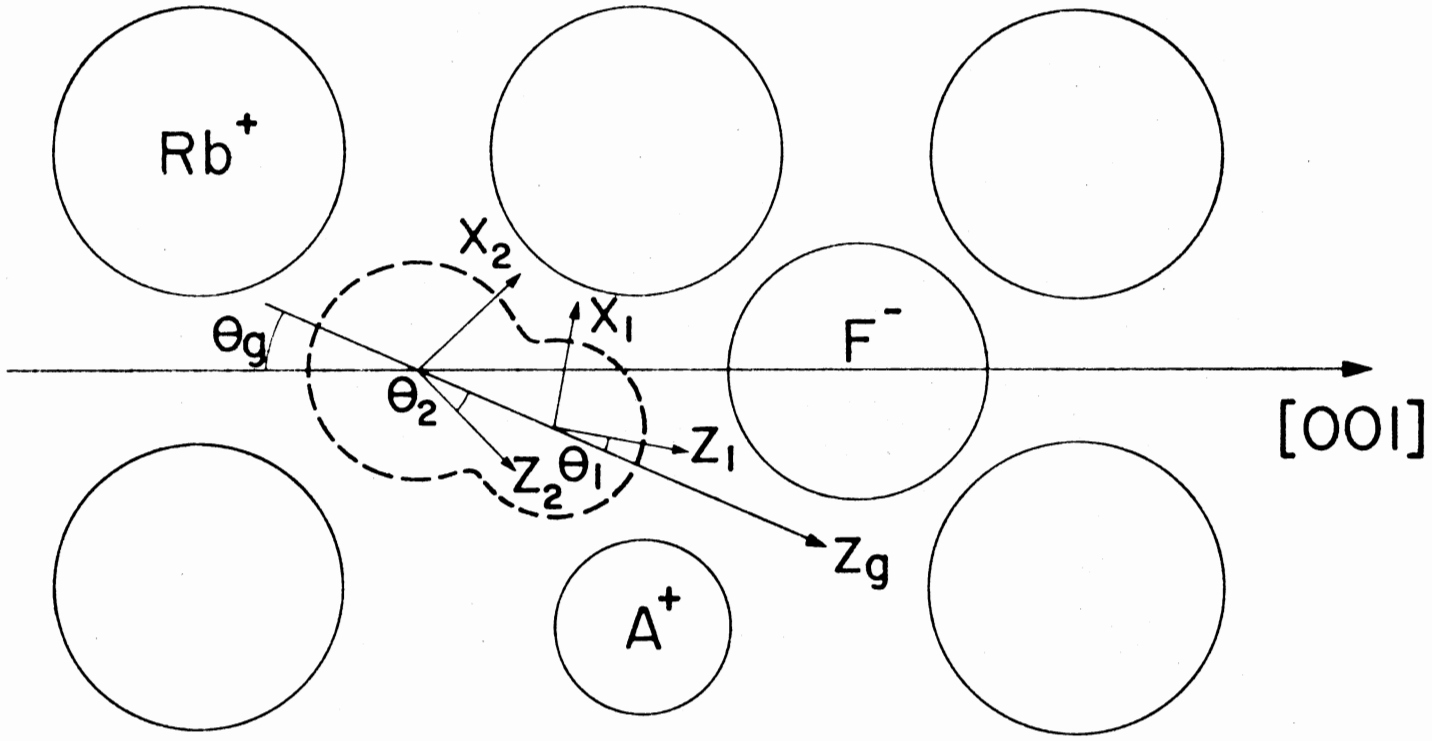

Figure 18. Schematic Representation and Orientations of the Three Principal Axes Coordinate Systems Pertinent to the $\overleftrightarrow{g}$, $\overleftrightarrow{A}_1$ and $\overleftrightarrow{A}_2$ Tensors

For site B $$[T]_i = \begin{pmatrix} 0 & -\cos\theta_i & -\sin\theta_i \\ 1 & 0 & 0 \\ 0 & -\sin\theta_i & \cos\theta_i \end{pmatrix}$$

For site C $$[T]_i = \begin{pmatrix} \cos\theta_i & 0 & \sin\theta_i \\ 0 & 1 & 0 \\ -\sin\theta_i & 0 & \cos\theta_i \end{pmatrix}$$

For site D $$[T]_i = \begin{pmatrix} \cos\theta_i & 0 & -\sin\theta_i \\ 0 & 1 & 0 \\ \sin\theta_i & 0 & \cos\theta_i \end{pmatrix}$$

In the above matrices, i = g represents $\overleftrightarrow{g}$ tensor, i = 1 represents $\overleftrightarrow{A}_1$ tensor and i = 2 represents $\overleftrightarrow{A}_2$ tensor. The transformation matrix [R] is defined the same as for the H centers.

Using the computer programs discussed in Chapter II, the spin Hamiltonian parameters of the H_A center were calculated to fit the measured line positions given in Table V. The final values of these parameters are given in Table VI. Using these values of parameters, the line positions were calculated and are given in Table V.

TABLE V

CALCULATED AND MEASURED LINE POSITIONS (IN GAUSS) OF THE H_A CENTER SPECTRUM

Direction of the magnetic field	Measured	Calculated
[001]	2395.90	2393.65
	3159.19	3157.84
	3404.92	3405.31
	4158.90	4160.68
[101]	2488.78	2489.78
	2582.35	2583.45
	2679.88*	2679.42
	3165.65	3166.98
	3179.85	3179.66
	3190.00	3191.41
	3355.45	3354.52
		3355.94
		3356.22
	3680.01	3677.47
	3828.44	3827.34
	3984.66	3982.74
[100]	2954.65	2954.90
	3110.12	3109.97
	3122.12	3121.99
	3229.73*	3229.72
	3249.78*	3253.61
	3264.59*	3266.28
		3278.67
	3343.66	3344.45

Microwave frequency = 9.2 GHz

* Not used in analysis.

TABLE VI

SPIN HAMILTONIAN PARAMETERS OF THE H_A CENTER IN $RbCaF_3$

g_x	2.0187 ± 0.0005
g_y	2.0173 ± 0.0005
g_z	2.0018 ± 0.0002
θ_g	$11.9^\circ \pm 0.2^\circ$
A_{1x}	268 ± 40 MHz
A_{1y}	261 ± 40 MHz
A_{1z}	2861 ± 3 MHz
θ_1	$2.5^\circ \pm 0.2^\circ$ (9.4° from [001])
A_{2x}	119 ± 40 MHz
A_{2y}	53 ± 40 MHz
A_{2z}	2192 ± 3 MHz
θ_2	$1.7^\circ \pm 0.2^\circ$ (13.6° from [001])

CHAPTER V

SUMMARY AND DISCUSSION

In the first part of this study, $[F_2^-]$ and H centers were produced in $RbCaF_3$ by electron irradiation at 77 K. Production study of these defects showed that the $[F_2^-]$ center saturates very fast while the H centers grow much more slowly with irradiation time. To study the H center, the $[F_2^-]$ center spectrum was first eliminated by bleaching the sample with ultraviolet light. Study of the remaining spectrum, which was due to the H center, revealed that the center consists of a negatively-charged fluorine molecular ion (two fluorines covalently bonded) replacing a normal fluorine ion and is oriented along the [001] axis. It was also found that the $RbCaF_3$ crystal was multidomain.

Using the measured magnetic fields corresponding to different H center lines and rigorous computer calculations, we were able to calculate the spin Hamiltonian parameters for this center. A thermal anneal study of the $[F_2^-]$ and H centers was done and the results showed that $[F_2^-]$ and H centers decay between 110 K and 150 K. At about 110 K a different set of lines were observed which grew until 150 K and then started to decay. This new center was found to be an H_A center. One of our goals was to study and characterize this center. To do this, the sample was warmed to 150 K after 77 K irradiation to produce the center and the spectrum was then observed at 77 K. Studies of the observed spectrum revealed that the H_A center also consists of a negatively-charged fluorine

molecular ion (two fluorines covalently bonded) replacing a normal fluorine ion but oriented with an angle with respect to [001] axis and the hole is more localized on the fluorine nearest to the impurity ion. Four possible orientations of H_A were found which is shown in Figure 13. Again, using the measured H_A lines we were able to calculate the corresponding spin Hamiltonian parameters.

The question arises as to why in the H and H_A centers in $RbCaF_3$ only two nuclei are involved while in $KMgF_3$, which has the same kind of basic crystal structure, more than two nuclei interact with the unpaired electron. The answer to this question lies in the fact that the $RbCaF_3$ has a larger lattice constant (4.45 A^o) as compared to $KMgF_3$ (3.97 A^o). This larger lattice constant means the distance between [110] nearest-neighbor fluorine is larger and there is less chance of interaction (reduced overlap integrals) between the unpaired electron and the outer fluorine nuclei. Actually, in this study of $RbCaF_3$ the interaction with these more distant neighbors was undetectable.

With regard to the optical measurements of Seretlo, Martin, and Sonder in $RbCaF_3$ (31), we were able to identify the observed bands to a higher degree of certainty. They observed three different absorption bands, at 320 nm, 400 nm, and 530 nm. We believe that the 320 nm band is due to the combination of $[F_2^-]$ and H centers. The fast initial rise in their growth curve versus irradiation dose is due to the $[F_2^-]$ center and corresponds to the fast rise in our production study of $[F_2^-]$ centers. The slower rise in their growth study for the 320 nm band corresponds to the slower rise in our production study of H centers. Their anneal study also shows that the 320 nm band anneals between about 100 K and 150 K which is the same as in our annealing study of both the $[F_2^-]$ and

H centers. It should be mentioned that after annealing above 100 K, the H_A center could also contribute to the 320 nm absorption band.

The growth versus irradiation dose for the 400 nm absorption band in Seretlo's paper is very similar to that of H center in our production study and since the production of H centers is accompanied by the production of F centers, it might be reasonable to assume that the 400 nm band is due to F centers. Unfortunately, the broad ESR spectral line of the F center does not allow their observation in this material.

There are additional research programs that can extend our understanding of the defect structure of $RbCaF_3$. ENDOR study of H_A centers can identify the stabilizing impurity. Optical studies of H and H_A centers can give us more information about their structure. The ESR studies of $RbCaF_3$ at liquid helium temperature might extend our knowledge about this material. The structure of $[\overline{F_2}]_A$ center in this material also remains to be studied.

SELECTED BIBLIOGRAPHY

1. Sonder, E., and W. A. Sibley, "Defect Creation by Radiation in Polar Crystals." Point Defects in Solids, Volume I, General and Ionic Crystals. J. H. Crawford, Jr., and L. M. Slifkin, eds. New York : Plenum Press, 1972, pp. 201-283.

2. Abragam, A., and B. Bleaney, Electron Paramagnetic Resonance of Transition Ions. Oxford: Clarendon Press, 1970.

3. Seidel, H., and H. C. Wolf, Physics of Color Centers, edited by W. B. Fowler, Academic Press,1968.

4. Sibley, W. A., and D. Pooley. "Radiation Studies of Materials Using Color Centers." Treatise on Materials Science and Technology, Volume 5. Academic Press, 1974.

5. Kanzig, W. and T. O. Woodruff, J. Phys. Chem. Solids 9, 70 (1958).

6. Compton, W. D., and C. C. Klick, Phys. Rev. 110, 349 (1958).

7. Nadeau, J. S., J. Appl. Phys. 33, 3480 (1962).

8. Sibley, W. A., and E. Sonder, J. Appl. Phys. 34, 2366 (1963).

9. Sibley, W. A., and J. R. Russell,J. Appl. Phys. 36, 810 (1965).

10. Balzer, R., H. Peisl, and W. Waidelich, Phys. Status Solidi 28, 207 (1968).

11. Balzer, R., H. Peisl, and W. Waidelich, Phys. Lett. A 27, 31 (1968).

12. Crawford, J. H., Advan. Phys. 17, 93 (1968).

13. Kabler, M. N., Phys. Rev. A 136, 1296 (1964).

14. Hall, T. P. P., D. Pooley, and P. T. Wedepohl, Proc. Phys. Soc., London 83, 635 (1964).

15. Pooley, D., Proc. Phys. Soc., London 89, 723 (1966).

16. Pooley, D., Proc. Phys. Soc., London 87, 245, 257 (1966).

17. Chu, Y. H., and R. L. Mieher, Phys. Rev. Letters, 20, 1289 (1968).

18. Chu, Y. H., and R. L. Mieher, Phys. Rev. 188, 1311 (1969).

19. Delbecq, C. J., E. Hutchinson, D. Schoemaker, E. L. Yasaitis, and P. H. Yuster, Phys. Rev. 187, 1103 (1969).

20. Patten, F. W., and F. J. Keller, Phys. Rev. 187, 1120 (1969).

21. Schoemaker, D., and J. L. Kolopus, Phys. Rev. B 2,1148 (1970).

22. Plant, W. J., and R. L. Mieher, Phys. Rev. B 7, 4793 (1973).

23. Riley, C. R., and W. A. Sibley, Phys. Rev. B 1, 2789 (1970).

24. Rose, B. H., J. E. Rhoads, and L. E. Halliburton, Phys. Rev. B 14, 3583 (1976).

25. Rhoads, J. E., B. H. Rose, and L. E. Halliburton, Phys. Rev. B 11, 5115 (1975).

26. Modine, F. A., E. Sonder, and W. P. Unruh, Phys. Rev. B 10, 1623 (1974).

27. Bates, J. B., R. W. Major, and F. A. Modine, Solid State Com. 17, 1347 (1975).

28. Ho, J. C., and W. P. Unruh, Phys. Rev. B 13, 447 (1976).

29. Halliburton, L. E., and E. Sonder, Solid State Com. 21, 445 (1977).

30. Maetz, J., M. Mullner, and H. Jex, Solid State Com. 28, 555 (1978).

31. Seretlo, J. R., J. J. Martin, and E. Sonder, Phys. Rev. B 14, 5405 (1976).

32. Burris, R. A., "Electron Spin Resonance Study of H Centers in $RbCaF_3$" (Unpub. M.S. Thesis, Oklahoma State University, 1978).

33. Wertz, J. E., and J. R. Bolton, Electron Spin Reonance: Elementary Theory and Practical Applications. New York: McGraw-Hill Book Company, 1973.

APPENDIXES

APPENDIX A

LISTING OF THE LINE POSTION PROGRAM

```
      IMPLICIT REAL*8 (A-H,O-Z)
      REAL I1,I2
      REAL*8 P(12),TG(3,3),T1(3,3),T2(3,3),R(3,3),TRG(3,3),TR1(3,3),TR2(
     &3,3),AR(8,8),AI(8,8),HF(4),D(8),E(8),E2(8),TAJ(2,8)
      P(1)=2.033D0
      P(2)=2.026D0
      P(3)=2.0018D0
      P(4)=5.08D2
      P(5)=5.42D2
      P(6)=3.1186D3
      P(7)=1.8172D2
      P(8)=1.932D2
      P(9)=1.6782D3
      P(10)=1.2D1
      P(11)=1.24D1
      P(12)=2.23D1
      WRITE (6,1) (P(I),I = 1,12)
    1 FORMAT ('0',/,'0',6F18.5)
      GBN = 5.6446D1/1.4092D4
      B = 9.2741D0/6.6262D0
      FREQQ=9.0996703
      DO 2 L = 10,12
    2 P(L) = P(L) * (3.14159D0/1.8D2)
      THETA = 0.D0
      PHI = 0.D0
    3 THETAR = THETA * (3.14159D0/1.8D2)
      PHIR = PHI * (3.14159D0/1.8D2)
      WRITE (6,4) THETA,PHI
    4 FORMAT ('0',2F15.3)
      R(1,1) = DCOS(THETAR)
      R(1,2) = -DSIN(THETAR) * DSIN(PHIR)
      R(1,3) = DSIN(THETAR) * DCOS(PHIR)
      R(2,1) = 0.D0
      R(2,2) = DCOS(PHIR)
      R(2,3) = DSIN(PHIR)
      R(3,1) = -DSIN(THETAR)
      R(3,2) = -DCOS(THETAR) * DSIN(PHIR)
      R(3,3) = DCOS(THETAR) * DCOS(PHIR)
      KK=1
    5 DO 6 L = 1,3
      DO 6 M = 1,3
      TG(L,M)=0.D0
      T1(L,M)=0.D0
    6 T2(L,M)=0.D0
      GO TO (7,8,9,10),KK
    7 AG = P(10)
      A1 = P(11)
      A2 = P(12)
      GO TO 11
    8 AG = -P(10)
      A1 = -P(11)
      A2 = -P(12)
      GO TO 11
    9 AG = P(10)
```

```
      A1 = P(11)
      A2 = P(12)
      GO TO 12
   10 AG = -P(10)
      A1 = -P(11)
      A2 = -P(12)
      GO TO 12
   11 TG(1,2) = -DCOS(AG)
      TG(1,3) = DSIN(AG)
      TG(2,1) = 1.D0
      TG(3,2) = DSIN(AG)
      TG(3,3) = DCOS(AG)
      T1(1,2) = -DCOS(A1)
      T1(1,3) = DSIN(A1)
      T1(2,1) = 1.D0
      T1(3,2) = DSIN(A1)
      T1(3,3) = DCOS(A1)
      T2(1,2) = -DCOS(A2)
      T2(1,3) = DSIN(A2)
      T2(2,1) = 1.D0
      T2(3,2) = DSIN(A2)
      T2(3,3) = DCOS(A2)
      GO TO 13
   12 TG(1,1) = DCOS(AG)
      TG(1,3) = DSIN(AG)
      TG(2,2) = 1.D0
      TG(3,1) = -DSIN(AG)
      TG(3,3) = DCOS(AG)
      T1(1,1) = DCOS(A1)
      T1(1,3) = DSIN(A1)
      T1(2,2) = 1.D0
      T1(3,1) = -DSIN(A1)
      T1(3,3) = DCOS(A1)
      T2(1,1) = DCOS(A2)
      T2(1,3) = DSIN(A2)
      T2(2,2) = 1.D0
      T2(3,1) = -DSIN(A2)
      T2(3,3) = DCOS(A2)
   13 DO 14 L = 1,3
      DO 14 M = 1,3
      TRG(L,M) = TG(L,1)*R(1,M) + TG(L,2)*R(2,M) + TG(L,3)*R(3,M)
      TR1(L,M) = T1(L,1)*R(1,M) + T1(L,2)*R(2,M) + T1(L,3)*R(3,M)
   14 TR2(L,M) = T2(L,1)*R(1,M) + T2(L,2)*R(2,M) + T2(L,3)*R(3,M)
      IA=1
   15 H = 3.0D3
   16 W1 = B*H*(P(1)*TRG(1,3)*TRG(1,1) + P(2)*TRG(2,3)*TRG(2,1) + P(3)*
     &TRG(3,3)*TRG(3,1))
      W2 = B*H*(P(1)*TRG(1,3)*TRG(1,2) + P(2)*TRG(2,3)*TRG(2,2) + P(3)*
     &TRG(3,3)*TRG(3,2))
      W3 = B*H*(P(1)*TRG(1,3)*TRG(1,3) + P(2)*TRG(2,3)*TRG(2,3) + P(3)*
     &TRG(3,3)*TRG(3,3))
      W4 = P(4)*TR1(1,1)*TR1(1,1) + P(5)*TR1(2,1)*TR1(2,1) + P(6)*TR1(3,
     &1)*TR1(3,1)
      W5 = P(4)*TR1(1,1)*TR1(1,2) + P(5)*TR1(2,1)*TR1(2,2) + P(6)*
```

```
     &TR1(3,1)*TR1(3,2)
      W6 = P(4)*TR1(1,1)*TR1(1,3) + P(5)*TR1(2,1)*TR1(2,3) + P(6)*
     &TR1(3,1)*TR1(3,3)
      W7= P(4)*TR1(1,2)*TR1(1,2) + P(5)*TR1(2,2)*TR1(2,2) + P(6)*TR1(3,2
     &)*TR1(3,2)
      W8 = P(4)*TR1(1,2)*TR1(1,3) + P(5)*TR1(2,2)*TR1(2,3) + P(6)*
     &TR1(3,2)*TR1(3,3)
      W9 = P(4)*TR1(1,3)*TR1(1,3) + P(5)*TR1(2,3)*TR1(2,3) + P(6)*
     &TR1(3,3)*TR1(3,3)
      W10 = P(7)*TR2(1,1)*TR2(1,1) + P(8)*TR2(2,1)*TR2(2,1) + P(9)*
     & TR2(3,1)*TR2(3,1)
      W11 = P(7)*TR2(1,1)*TR2(1,2) + P(8)*TR2(2,1)*TR2(2,2) + P(9)*
     &TR2(3,1)*TR2(3,2)
      W12 = P(7)*TR2(1,1)*TR2(1,3) + P(8)*TR2(2,1)*TR2(2,3) + P(9)*
     &TR2(3,1)*TR2(3,3)
      W13 = P(7)*TR2(1,2)*TR2(1,2) + P(8)*TR2(2,2)*TR2(2,2) + P(9)*
     &TR2(3,2)*TR2(3,2)
      W14 = P(7)*TR2(1,2)*TR2(1,3) + P(8)*TR2(2,2)*TR2(2,3) + P(9)*
     &TR2(3,2)*TR2(3,3)
      W15 = P(7)*TR2(1,3)*TR2(1,3) + P(8)*TR2(2,3)*TR2(2,3) + P(9)*
     &TR2(3,3)*TR2(3,3)
      Q1R = W1/2.D0
      Q1I = W2/2.D0
      Q2R = (W4-W7)/4.D0
      Q2I = W5/2.D0
      Q3 = (W4 + W7)/4.D0
      Q4R = W6/2.D0
      Q4I = W8/2.D0
      Q5R = (W10-W13)/4.D0
      Q5I = W11/2.D0
      Q6 = (W10 + W13)/4.D0
      Q7R = W12/2.D0
      Q7I = W14/2.D0
      I1=0.5D0
      I2=0.5D0
      AB=2.D0*I1+1.D0
      AC=2.D0*I2+1.D0
      A=AB*AC
      AA=2.D0*A
      K=AA
      DO 119 L=1,K
      DO 119 M=1,K
      AR(L,M)=0.D0
  119 AI(L,M)=0.D0
      K=AB
      I=AC
      DO 205 L=1,K
      K1=AB+1.D0-2.D0*L
      DO 205 M=1,I
      K2=AC+1.D0-2.D0*M
      J=L*M+(L-1)*(AC-M)
      AR(J,J)=W3/2.D0+W9*K1/4.D0+W15*K2/4.D0-GBN*H*(K1+K2)/2.D0
      N=J+A
  120 AR(N,N)=-W3/2.D0-W9*K1/4.D0-W15*K2/4.D0-GBN*H*(K1+K2)/2.D0
```

```
      N=J+A
      AR(N,J)=Q1R+Q4R*K1/2.D0+Q7R*K2/2.D0
      AI(N,J)=Q1I+Q4I*K1/2.D0+Q7I*K2/2.D0
      N=J+1
      IF(L.EQ.K.AND.M.EQ.I)GO TO 200
      AR(N,J)=0.5D0*Q7R*DSQRT((I2+K2/2.D0)*(I2-K2/2.D0+1.D0))
      AI(N,J)=0.5D0*Q7I*DSQRT((I2+K2/2.D0)*(I2-K2/2.D0+1.D0))
      NN=J+A+1
      NM=J+A
      AR(NN,NM)=-AR(N,J)
  121 AI(NN,NM)=-AI(N,J)
      N=J+A+1
      AR(N,J)=Q5R*DSQRT((I2+K2/2.D0)*(I2-K2/2.D0+1.D0))
  125 AI(N,J)=Q5I*DSQRT((I2+K2/2.D0)*(I2-K2/2.D0+1.D0))
  200 CONTINUE
      IF(L.EQ.K) GO TO 202
      N=J+AC
       AR(N,J)=0.5D0*Q4R*DSQRT((I1-K1/2.D0+1.D0)*(I1+K1/2.D0))
       AI(N,J)=0.5D0*Q4I*DSQRT((I1-K1/2.D0+1.D0)*(I1+K1/2.D0))
      NA=J+AC+A
      JA=J+A
      AR(NA,JA)=-AR(N,J)
  122 AI(NA,JA)=-AI(N,J)
      IF(I1.GT.0.5) GO TO 201
      IF(I2.GT.0.5) GO TO 201
      AR(5,3)=Q3
      AR(6,4)=Q3
  201 CONTINUE
      N=J+A+AC
      AR(N,J)=Q2R*DSQRT((I1-K1/2.D0+1.D0)*(I1+K1/2.D0))
  126 AI(N,J)=Q2I*DSQRT((I1-K1/2.D0+1.D0)*(I1+K1/2.D0))
  202 CONTINUE
  205 CONTINUE
      DO 124 M=1,I
      K2=AC+1.DC-2.D0*M
      J=M
      N=J+A
      NN=J+1
      AR(N,NN)=Q6 *DSQRT((I2-K2/2.D0+1.D0)*(I2+K2/2.D0))
      NA=AB-1.D0
      DO 124 NJ=1,NA
      NK=N+NJ*AC
      NP=NN+NJ*AC
  124 AR(NK,NP)=AR(N,NN)
      N = 8
      NM = 8
      CALL HTRIDI (NM,N,AR,AI,D,E,E2,TAU)
      CALL IMTQL1 (N,D,E,IERR)
      FREQ=D(9-IA)-D(IA)
      IF (DABS(FREQQ-FREQ) - 1.D0) 18,18,19
   18 HF(IA)=H
      GO TO 20
   19 H = H*(FREQQ/FREQ)
      GO TO 16
```

```
217      20   IF( IA-4)21,22,22
218      21   IA= IA+1
219           GO TO 15
220      22   WRITE( 6, 23)( HF( IA ), IA= 1, 4)
221       23 FORMAT (4F20.2)
222           IF (KK-4) 24,25,25
223      24   KK=KK+1
224           GO TO 5
225       25 THETA = THETA+ 5.D0
226           IF (THETA - 9.1D1) 3, 26, 26
227       26 CONTINUE
228           STOP
229           END
```

APPENDIX B

LISTING OF THE FITTING PROGRAM

```
      IMPLICIT REAL*8 (A-H,O-Z)
      REAL*8 P(12),TG(3,3),T1(3,3),T2(3,3),R(3,3),TRG(3,3),TR1(3,3),TR2(
     &3,3),AR(8,8),AI(8,8),HF(4),D(8),E(8),E2(8),TAU(2,8),FREQ1(21)
      P(1)=2.0187D0
      P(2)=2.0176D0
      P(3)=2.0018D0
      P(4)=2.63D2
      P(5)=2.56D2
      P(6)=2.862D3
      P(7)=1.31D2
      P(8)=5.6D1
      P(9)=2.19D3
      P(10)=1.19D1
      P(11)=9.4D0
      P(12)=1.36D1
      WRITE(6,1) (P(I),I=1,12)
    1 FORMAT('0',/,'0',6F18.5)
      GBN=5.64460D1/1.4092D4
      B=9.2741D0/6.6262D0
      FREQQ=9.2D3
      DO 2 L=10,12
    2 P(L)=P(L)*(3.14159D0/1.8D2)
      PHI=0.0D0
   40 DO 35 LL=1,12
   41 K1=1
   42 MM=1
   43 GO TO (44,45,46,47,48,49,50,51,52,53,54,55,56,57,58,59,60,61,62,63
     1,64),MM
   44 H=2.3959D3
      THETA=0.0D0
      K=1
      I=1
      GO TO 3
   45 H=3.1591D3
      I=2
      GO TO 3
   46 H=3.4049ZD3
      I=3
      GO TO 3
   47 H=4.1589D3
      I=4
      GO TO 3
   48 H=2.4887D3
      THETA=4.5D1
      K=4
      I=1
      GO TO 3
   49 H=2.5823D3
      K=1
      GO TO 3
   50 H=2.6798D3
      K=3
      GO TO 3
   51 H=3.1656D3
```

```
      K=3
      I=2
      GO TO 3
   52 H=3.17985D3
      K=1
      I=2
      GO TO 3
   53 H=3.19D3
      K=4
      I=2
      GO TO 3
   54 H=3.35545D3
      K=1
      I=3
      GO TO 3
   55 H=3.68001D3
      K=3
      I=4
      GO TO 3
   56 H=3.82844D3
      K=1
      GO TO 3
   57 H=3.98466D3
      K=4
      GO TO 3
   58 H=3.35545D3
      K=3
      I=3
      GO TO 3
   59 H=3.35545D3
      K=4
      I=3
      GO TO 3
   60 H=2.95465D3
      THETA=9.D1
      K=3
      I=1
      GO TO 3
   61 H=3.11012D3
      K=1
      I=1
      GO TO 3
   62 H=3.12212D3
      I=2
      GO TO 3
   63 H=3.22973D3
      K=4
      I=2
      GO TO 3
   64 H=3.34366D3
      K=3
      I=4
    3 THETAR = THETA * (3.14159D0/1.8D2)
      PHIR = PHI * (3.14159D0/1.8D2)
```

```
      R(1,1) = DCOS(THETAR)
      R(1,2) = -DSIN(THETAR) * DSIN(PHIR)
      R(1,3) = DSIN(THETAR) * DCOS(PHIR)
      R(2,1) = 0.D0
      R(2,2) = DCOS(PHIR)
      R(2,3) = DSIN(PHIR)
      R(3,1) = -DSIN(THETAR)
      R(3,2) = -DCOS(THETAR) * DSIN(PHIR)
      R(3,3) = DCOS(THETAR) * DCOS(PHIR)
    5 DO 6 L = 1,3
      DO 6 M = 1,3
      TG(L,M) = 0.D0
      T1(L,M) = 0.D0
    6 T2(L,M) = 0.D0
      GO TO (7,8,9,10),K
    7 AG = P(10)
      A1 = P(11)
      A2 = P(12)
      GO TO 11
    8 AG = -P(10)
      A1 = -P(11)
      A2 = -P(12)
      GO TO 11
    9 AG = P(10)
      A1 = P(11)
      A2 = P(12)
      GO TO 12
   10 AG = -P(10)
      A1 = -P(11)
      A2 = -P(12)
      GO TO 12
   11 TG(1,2) = -DCOS(AG)
      TG(1,3) = DSIN(AG)
      TG(2,1) = 1.D0
      TG(3,2) = DSIN(AG)
      TG(3,3) = DCOS(AG)
      T1(1,2) = -DCOS(A1)
      T1(1,3) = DSIN(A1)
      T1(2,1) = 1.D0
      T1(3,2) = DSIN(A1)
      T1(3,3) = DCOS(A1)
      T2(1,2) = -DCOS(A2)
      T2(1,3) = DSIN(A2)
      T2(2,1) = 1.D0
      T2(3,2) = DSIN(A2)
      T2(3,3) = DCOS(A2)
      GO TO 13
   12 TG(1,1) = DCOS(AG)
      TG(1,3) = DSIN(AG)
      TG(2,2) = 1.D0
      TG(3,1) = -DSIN(AG)
      TG(3,3) = DCOS(AG)
      T1(1,1) = DCOS(A1)
      T1(1,3) = DSIN(A1)
```

```
      T1(2,2) = 1.D0
      T1(3,1) = -DSIN(A1)
      T1(3,3) = DCOS(A1)
      T2(1,1) = DCOS(A2)
      T2(1,3) = DSIN(A2)
      T2(2,2) = 1.D0
      T2(3,1) = -DSIN(A2)
      T2(3,3) = DCOS(A2)
   13 DO 14 L = 1,3
      DO 14 M = 1,3
      TRG(L,M) = TG(L,1)*R(1,M) + TG(L,2)*R(2,M) + TG(L,3)*R(3,M)
      TR1(L,M) = T1(L,1)*R(1,M) + T1(L,2)*R(2,M) + T1(L,3)*R(3,M)
   14 TR2(L,M) = T2(L,1)*R(1,M) + T2(L,2)*R(2,M) + T2(L,3)*R(3,M)
   16 W1 = B*H*(P(1)*TRG(1,3)*TRG(1,1) + P(2)*TRG(2,3)*TRG(2,1) + P(3)*
     &TRG(3,3)*TRG(3,1))
      W2 = B*H*(P(1)*TRG(1,3)*TRG(1,2) + P(2)*TRG(2,3)*TRG(2,2) + P(3)*
     &TRG(3,3)*TRG(3,2))
      W3 = B*H*(P(1)*TRG(1,3)*TRG(1,3) + P(2)*TRG(2,3)*TRG(2,3) + P(3)*
     &TRG(3,3)*TRG(3,3))
      W4 = P(4)*TR1(1,1)*TR1(1,1) + P(5)*TR1(2,1)*TR1(2,1) + P(6)*TR1(3,
     &1)*TR1(3,1)
      W5 = P(4)*TR1(1,1)*TR1(1,2) + P(5)*TR1(2,1)*TR1(2,2) + P(6)*
     &TR1(3,1)*TR1(3,2)
      W6 = P(4)*TR1(1,1)*TR1(1,3) + P(5)*TR1(2,1)*TR1(2,3) + P(6)*
     &TR1(3,1)*TR1(3,3)
      W7= P(4)*TR1(1,2)*TR1(1,2) + P(5)*TR1(2,2)*TR1(2,2) + P(6)*TR1(3,2
     &)*TR1(3,2)
      W8 = P(4)*TR1(1,2)*TR1(1,3) + P(5)*TR1(2,2)*TR1(2,3) + P(6)*
     &TR1(3,2)*TR1(3,3)
      W9 = P(4)*TR1(1,3)*TR1(1,3) + P(5)*TR1(2,3)*TR1(2,3) + P(6)*
     &TR1(3,3)*TR1(3,3)
      W10 = P(7)*TR2(1,1)*TR2(1,1) + P(8)*TR2(2,1)*TR2(2,1) + P(9)*
     &TR2(3,1)*TR2(3,1)
      W11 = P(7)*TR2(1,1)*TR2(1,2) + P(8)*TR2(2,1)*TR2(2,2) + P(9)*
     &TR2(3,1)*TR2(3,2)
      W12 = P(7)*TR2(1,1)*TR2(1,3) + P(8)*TR2(2,1)*TR2(2,3) + P(9)*
     &TR2(3,1)*TR2(3,3)
      W13 = P(7)*TR2(1,2)*TR2(1,2) + P(8)*TR2(2,2)*TR2(2,2) + P(9)*
     &TR2(3,2)*TR2(3,2)
      W14 = P(7)*TR2(1,2)*TR2(1,3) + P(8)*TR2(2,2)*TR2(2,3) + P(9)*
     &TR2(3,2)*TR2(3,3)
      W15 = P(7)*TR2(1,3)*TR2(1,3) + P(8)*TR2(2,3)*TR2(2,3) + P(9)*
     &TR2(3,3)*TR2(3,3)
      Q1R = W1/2.D0
      Q1I = W2/2.D0
      Q2R = (W4-W7)/4.D0
      Q2I = W5/2.D0
      Q3 = (W4 + W7)/4.D0
      Q4R = W6/2.D0
      Q4I = W8/2.D0
      Q5R = (W10-W13)/4.D0
      Q5I = W11/2.D0
      Q6 = (W10 + W13)/4.D0
      Q7R = W12/2.D0
```

```
      Q7I = W14/2.D0
      I1=0.5D0
      I2=0.5D0
      AB=2.D0*I1+1.D0
      AC=2.D0*I2+1.D0
      A=AB*AC
      AA=2.D0*A
      KA=AA
      DO 119 L=1,KA
      DO 119 M=1,KA
      AR(L,M)=0.D0
  119 AI(L,M)=0.D0
      KA=AB
      IK=AC
      DO 205 L=1,KA
      K1=AB+1.D0-2.D0*L
      DO 205 M=1,IK
      K2=AC+1.D0-2.D0*M
      J=L*M+(L-1)*(AC-M)
      AR(J,J)=W3/2.D0+W9*K1/4.D0+W15*K2/4.D0-GBN*H*(K1+K2)/2.D0
      N=J+A
  120 AR(N,N)=-W3/2.D0-W9*K1/4.D0-W15*K2/4.D0-GBN*H*(K1+K2)/2.D0
      N=J+A
      AR(N,J)=Q1R+Q4R*K1/2.D0+Q7R*K2/2.D0
      AI(N,J)=Q1I+Q4I*K1/2.D0+Q7I*K2/2.D0
      N=J+1
      IF(L.EQ.KA.AND.M.EQ.IK) GO TO 200
      AR(N,J)=0.5D0*Q7R*DSQRT((I2+K2/2.D0)*(I2-K2/2.D0+1.D0))
      AI(N,J)=0.5D0*Q7I*DSQRT((I2+K2/2.D0)*(I2-K2/2.D0+1.D0))
      NN=J+A+1
      NM=J+A
      AR(NN,NM)=-AR(N,J)
  121 AI(NN,NM)=-AI(N,J)
      N=J+A+1
      AR(N,J)=Q5R*DSQRT((I2+K2/2.D0)*(I2-K2/2.D0+1.D0))
  125 AI(N,J)=Q5I*DSQRT((I2+K2/2.D0)*(I2-K2/2.D0+1.D0))
  200 CONTINUE
      IF(L.EQ.KA) GO TO 202
      N=J+AC
       AR(N,J)=0.5D0*Q4R*DSQRT((I1-K1/2.D0+1.D0)*(I1+K1/2.D0))
       AI(N,J)=0.5D0*Q4I*DSQRT((I1-K1/2.D0+1.D0)*(I1+K1/2.D0))
      NA=J+AC+A
      JA=J+A
      AR(NA,JA)=-AR(N,J)
  122 AI(NA,JA)=-AI(N,J)
      IF(I1.GT.0.5) GO TO 201
      IF(I2.GT.0.5) GO TO 201
      AR(5,3)=Q3
      AR(6,4)=Q3
  201 CONTINUE
      N=J+A+AC
      AR(N,J)=Q2R*DSQRT((I1-K1/2.D0+1.D0)*(I1+K1/2.D0))
  126 AI(N,J)=Q2I*DSQRT((I1-K1/2.D0+1.D0)*(I1+K1/2.D0))
  202 CONTINUE
```

```
  205  CONTINUE
       DO 124 M=1,IK
       K2=AC+1.DO-2.DO*M
       J=M
       N=J+A
       NN=J+1
       AR(N,NN)=Q6 *DSQRT((I2-K2/2.DO+1.DO)*(I2+K2/2.DO))
       NA=AB-1.DO
       DO 124 NJ=1,NA
       NK=N+NJ*AC
       NP=NN+NJ*AC
  124  AR(NK,NP)=AR(N,NN)
       N=8
       NM=8
       CALL HTRIDI (NM,N,AR,AI,D,E,E2,TAU)
       CALL IMTQL1 (N,D,E,IERR)
       FREQ1(MM)=D(9-I)-D(I)
       MM=MM+1
       IF (MM-21) 43,43,22
   22  SUM=0.DO
       DO 23 MM=1,21
   23  SUM=SUM+(FREQ1(MM)-FREQ0)**2
       GO TO (24,31,33),K1
   24  SUM2=SUM
       IF (LL-1) 25,25,26
   25  SUM1=SUM
   26  GO TO (27,27,27,28,28,28,28,28,28,29,29,29),LL
   27  PP=1.0D-4
       GO TO 30
   28  PP=1.0D0
       GO TO 30
   29  PP=1.0D-1*(3.14159D0/1.802)
   30  P(LL)=P(LL)+PP
       K1=K1+1
       GO TO 42
   31  IF (SUM-SUM2) 35,32,32
   32  P(LL)=P(LL)-2.DO*PP
       K1=K1+1
       GO TO 42
   33  IF (SUM-SUM2) 35,34,34
   34  P(LL)=P(LL)+PP
   35  CONTINUE
       IF (SUM-SUM2) 36,37,37
   36  SUM2=SUM
   37  CONTINUE
       WRITE(6,38)SUM2
   38  FORMAT (' SUM2 EQUALS',F12.3)
       WRITE(6,39) (P(I),I=1,12)
   39  FORMAT ('0',12F11.5)
       IF(SUM1-SUM2) 90,90,40
   90  CONTINUE
       STOP
       END
```

VITA

Anooshirvan Jafari

Candidate for the Degree of

Doctor of Philosophy

Thesis: INVESTIGATION OF RADIATION-INDUCED INTERSTITIALS IN $RbCaF_3$

Major Field: Physics

Biographical:

Personal Data: Born in Arak, Iran, November 28, 1945, the son of Mr. and Mrs. Ahmad Jafari.

Education: Graduated from Marvi High School, Tehran, Iran, in May, 1963; received Bachelor of Science degree in Physics from Tehran University, Tehran, Iran, in 1966; received Master of Science degree in Physics from Pahlavi University, Shiraz, Iran, in 1969; received Master of Science degree in Physics from Indiana University, Bloomington, Indiana, in 1974; completed the requirements for the degree of Doctor of Philosophy at Oklahoma State University, in July, 1980.

Professional Experience: Employed as teaching assistant (1966-69) and Instructor (1969-70) in the Physics Department of Pahlavi University, Shiraz, Iran; teaching assistant in the Physics Department of Indiana University, Bloomington, Indiana (1971-74); Instructor in the Physics Department of Ferdowsi University, Mashhad, Iran (1974-76); teaching and research assistant in the Physics Department of Oklahoma State University, Stillwater, Oklahoma (1978-80).